

ABSTRACT

CAO, PETER XUAN. Effects of Nanoconfinement in Anodized Aluminum Oxide on Structure and Alignment of Lipid Membranes under Dehydration Conditions. (Under the Direction of Prof. Alex I. Smirnov).

Lipid membranes are highly sensitive to dehydration, typically losing structural order and functionality when water is removed. In this work, we demonstrate that nanoconfinement within anodic aluminum oxide (AAO) nanopores provides a robust physical scaffold that preserves membrane alignment and integrity under conditions that destabilize bulk vesicles. Using X-band EPR spectroscopy with spin-labeled lipids, we show that DPPC bilayers confined in AAO exhibit macroscopic alignment across the gel-to-liquid crystalline transition, an effect absent in bulk systems. Dehydration experiments revealed that although lipid alignment diminishes in the absence of additives, lipid confinement in AAO provides for a residual degree of order, enabling recovery of lipid bilayers upon rehydration. Small molecular size sugars such as Trehalose further enhanced lipid bilayer stability, preserving lipid alignment in fully dehydrated membranes by substituting for hydration shells at lipid headgroups, while large molecular size sugars such as Ficoll have no protective effect. Comparative studies of DPPC and DOPC highlighted the importance of lipid phase state, with fluid membranes displaying greater resilience under nanoconfinement. Measurements of inter-residue distances in gramicidin A dimers by double electron electron resonance (DEER) confirmed the persistence of dimeric transmembrane channel in AAO-confined, trehalose-stabilized membranes even under dehydration. Together, these results establish AAO nanoconfinement as a powerful tool for maintaining membrane order and function over a broad range of environmental conditions including dehydration, with potential applications in nanostructured biointerfaces, cryoprotection, and membrane protein stabilization.

Effects of Nanoconfinement in Anodized Aluminum Oxide on Structure and
Alignment of Lipid Membranes under Dehydration Conditions

by

Peter Xuan Cao

A thesis submitted to the Graduate Faculty of

North Carolina State University

in partial fulfillment of the

Requirements for the Degree of

Master of Science

Chemistry

Raleigh, North Carolina

2025

APPROVED BY:

Prof. Thomas Theis

Prof. Alexander Nevzorov

Prof. Alex Smirnov

Chair of Advisory Committee

ACKNOWLEDGEMENTS

I would like to thank God for giving me the strength, courage, and wisdom to endure these past 2 years of graduate school. Next, I am grateful to my family (Cao Xuan Phuong, Vo Thi Na, Cao Xuan Mari Hong Hanh, Cao Xuan David, Cao Xuan Mary Hong Nhung) and my girlfriend (Le Thi Thuy) whose love and encouragement carried me through the most difficult. Then, I would like to express my sincere appreciation to Professor. Alex Smirnov for his invaluable guidance, mentorship, and support throughout my studies. His insight, dedication, and encouragement have greatly shaped both my research and my development as a scientist. Finally, I am thankful to all the members of the Smirnov/Smirnova and Nevzorov research group who have generously shared their knowledge, provided technical assistance and welcoming research environment.

TABLE OF CONTENTS

List of Figures..... vi

List of Tables..... ix

1. INTRODUCTION 1

1.1.	General introduction to lipid membranes.....	2
1.2.	Why lipid membrane structure is important for function.....	3
1.3.	Importance of lipid membrane hydration for stability of its structure.....	5
1.4.	Introduction to anodic aluminum oxide (AAO).....	6
1.5.	How AAO is used to study lipid membranes.....	7
1.6.	General introduction to EPR spectroscopy.....	8
1.6.1	Basic resonance condition.....	8
1.6.2	Spin Hamiltonian.....	8
1.6.3	CW EPR spectral information.....	9
1.6.4	Electron–electron dipolar coupling.....	10
1.6.5	CW vs Pulsed EPR.....	10
1.6.6	Pulsed EPR and DEER spectroscopy.....	11
1.6.7	Distance measurements.....	11
1.6.8	Four-pulse DEER.....	11
1.6.9	Data analysis.....	12
1.6.10	Developments.....	12
1.6.11	Spin-labeled lipids.....	12
1.6.12	Protein–lipid interactions.....	13
1.6.13	Structural insights from EPR.....	13
1.7.	Lipid Membrane Stability under Dehydration and the Role of AAO Nanostructured Supports.....	14

2. MATERIALS AND METHODS15

2.1	Materials.....	15
-----	----------------	----

2.2	Sample preparation	16
2.3	Preparation of AAO Nanopores Samples with DOPC (MLVs) or DPPC (MLVs)	17
2.4	Preparation of samples at different hydration Levels	18
2.5	Variable Temperature Experiments	20
2.6	X-band CW-EPR measurements	20
2.7	Pulsed Q-band (34GHz): DEER spectroscopy.....	20
2.8	Software Computer	21
3.	RESULTS	22
3.1	X-band EPR Characterization of Hydrated 5-DSA–Labeled DPPC Membranes Aligned Inside AAO Nanopores (Temperature= 23°C)	22
3.2	EPR Characterization of 5-DSA–Doped DPPC Membranes Embedded in AAO with/without Ficoll under Dehydration at (Temperature = 23°C).....	26
3.3	EPR Characterization of 5-DSA–Doped DPPC Membranes Embedded in AAO with Trehalose under Dehydration at (Temperature = 23°C).....	27
3.4	Humidity control inside AAO	30
3.4.1	Humidity-Dependent Behavior of 5-DSA–Labeled DPPC Membranes within AAO under Dehydration at 23 °C.....	30
3.4.2	Humidity-Dependent Behavior of 5-DSA–Labeled DOPC Membranes within AAO under Dehydration at 23°C.....	33
	Effect of the lipid structure on membrane integrity.....	33
3.4.3	DOPC: controlled humidity and no sugar added.	34
3.4.4	DOPC: controlled humidity and Trehalose added.	36
3.4.5	DPPC:5-DSA doped inside AAO nanopores at 50°C.....	38
3.5	Quantitative estimation of the structural order in dehydrated DOPC membranes using numerical simulations.....	40
3.6	Probing the dehydrated DOPC membrane structure globally: DEER spectroscopy of Gramicidin A protein.....	46

4. CONCLUSIONS	51
5. REFERENCES	53

LIST OF FIGURES

FIGURE 2.1 : COMPARISON UNDER UV ILLUMINATION OF GA–SPIN LABEL CONJUGATE (RIGHT) AND GA CONTROL (LEFT) IN THIN-LAYER CHROMATOGRAPHY.....	17
FIGURE 2.2 (A) SCHEMATIC REPRESENTATION OF NCSU-BUILT HUMIDITY-CONTROLLING SETUP FOR A SAMPLE INSIDE EPR CAVITY. (B) SAMPLES AAO WITH LIPID BILAYER INSIDE EPR CAVITY WITH AAO SURFACE PERPENDICULAR TO THE POLARIZING MAGNETIC FIELD.....	19
FIGURE 3.1 TEMPERATURE-DEPENDENT EPR SPECTRA OF AQUEOUS SUSPENSIONS OF DPPC MLVS DOPED WITH 1 MOL% 5-DOXYL STEARIC ACID (5-DSA) IN BUFFER SOLUTION (50MM HEPES, PH 7.0) AT 25 °C, 35 °C, 45 °C.....	22
FIGURE 3.2: A) CHEMICAL STRUCTURE OF TEMPOL (4-HYDROXY-2,2,6,6-TETRAMETHYLPYPERIDINE-1-OXYL) NITROXIDE. B) NITROXIDE AT 3D VIEW WITH THREE DIMENSIONS INCLUDING GXX,GYY AND GZZ. C) CHEMICAL STRUCTURE OF 16:0-5 DOXYL PC ((1-PALMITOYL-2-STEAROYL-(5-DOXYL)-SN-GLYCERO-3-PHOSPHOCHOLINE) LIPID CONTAINING DOXYL NITROXIDE AT THE POSITION 5TH OF ACYL CHAIN IN 2D. D) 16:0-5 DOXYL PC IN 3D. E) DPPC:5DSA ARE SELF-ASSEMBLING INSIDE AAO INTO CYLINDRICAL STRUCTURE WITH DOXYL Z-MAGNETIC AXIS (GZZ) PERPENDICULAR TO THE DIRECTION OF THE PORE THAT IS ALIGNED ALONG THE EXTERNAL MAGNETIC FIELD.....	24
FIGURE 3.3 EPR (X-BAND) SPECTRA OF DPPC MEMBRANES LABELED WITH 1 MOL% 5-DOXYL STEARIC ACID (5-DSA) INSIDE AAO ARE SELF-ASSEMBLING WITH HYDRATION CONDITIONS INCLUDING MAGNETIC AXIS WITH DOXYL (GZZ) PARALLEL (BLUE SPECTRUM) AND PERPENDICULAR (RED SPECTRUM) TO THE DIRECTION OF THE PORE THAT IS ALIGNED ALONG THE EXTERNAL MAGNETIC FIELD.....	25
FIGURE 3.4 X-BAND EPR SPECTRA OF DPPC MEMBRANES CONTAINING 1 MOL% 5-DOXYL STEARIC ACID (5DSA) SPIN LABELS CONFINED IN ANODIC ALUMINUM OXIDE (AAO) NANOPORES INSIDE AAO ARE SELF-ASSEMBLING WITH DEHYDRATION CONDITIONS AT ROOM TEMPERATURE (23°C) INCLUDING MAGNETIC AXIS WITH DOXYL (GZZ) PARALLEL (BLUE SPECTRUM) AND PERPENDICULAR (RED	

SPECTRUM) TO THE DIRECTION OF THE PORE THAT IS ALIGNED ALONG THE EXTERNAL MAGNETIC FIELD WITH (A) WITHOUT (B) WITH FICOLL..... 27

FIGURE 3.5 EPR (X-BAND) SPECTRA OF DPPC MEMBRANES LABELED WITH 1 MOL% 5-DOXYL STEARIC ACID (5-DSA) INSIDE AAO ARE SELF-ASSEMBLING WITH DEHYDRATION CONDITIONS INCLUDING MAGNETIC AXIS WITH DOXYL (GZZ) PARALLEL (**BLUE SPECTRUM**) AND **PERPENDICULAR (RED SPECTRUM)** TO THE DIRECTION OF THE PORE THAT IS ALIGNED ALONG THE EXTERNAL MAGNETIC FIELD AT (A) 23°C, (B) 50°C..... 30

FIGURE 3.6: EPR (X-BAND) SPECTRA OF **DPPC** MEMBRANES LABELED WITH 1 MOL% 5-DOXYL STEARIC ACID (5-DSA) INSIDE AAO ARE SELF-ASSEMBLING WITH A RANGE OF RELATIVE HUMIDITY CONDITIONS (10-95% RH) AT 23°C INSIDE EPR CAVITY INCLUDING MAGNETIC AXIS WITH DOXYL (GZZ) PARALLEL (**BLUE SPECTRUM**) AND **PERPENDICULAR (RED SPECTRUM)** TO THE DIRECTION OF THE PORE THAT IS ALIGNED ALONG THE EXTERNAL MAGNETIC FIELD..... 33

FIGURE 3.7 EPR (X-BAND) SPECTRA OF **DOPC** MEMBRANES LABELED WITH 1 MOL% 5-DOXYL STEARIC ACID (5-DSA) INSIDE AAO ARE SELF-ASSEMBLING WITH A RANGE OF RELATIVE HUMIDITY CONDITIONS (10-95% RH) AT 23°C INSIDE EPR CAVITY INCLUDING MAGNETIC AXIS WITH DOXYL (GZZ) PARALLEL (**BLUE SPECTRUM**) AND **PERPENDICULAR (RED SPECTRUM)** TO THE DIRECTION OF THE PORE THAT IS ALIGNED ALONG THE EXTERNAL MAGNETIC FIELD..... 36

FIGURE 3.8 EPR (X-BAND) SPECTRA OF **DOPC** MEMBRANES LABELED WITH 1 MOL% 5-DOXYL STEARIC ACID (5-DSA) ASSEMBLED WITHIN AAO AND STABILIZED WITH TREHALOSE 20% (W/V) SOLUTION. THE SPECTRUM WAS MEASURED UNDER A RANGE OF RELATIVE HUMIDITY CONDITIONS (10-95% RH) AT 23°C INSIDE EPR CAVITY INCLUDING MAGNETIC AXIS WITH DOXYL (GZZ) PARALLEL (**BLUE SPECTRUM**) AND **PERPENDICULAR (RED SPECTRUM)** TO THE DIRECTION OF THE PORE THAT IS ALIGNED ALONG THE EXTERNAL MAGNETIC FIELD.. 38

FIGURE 3.9 EPR (X-BAND) SPECTRA OF DPPC MEMBRANES LABELED WITH 1 MOL% 5-DOXYL STEARIC ACID (5-DSA) INSIDE AAO ARE SELF-ASSEMBLING WITH DEHYDRATION CONDITIONS INCLUDING MAGNETIC AXIS WITH DOXYL (GZZ) PARALLEL (**BLUE SPECTRUM**) AND **PERPENDICULAR (RED SPECTRUM)** TO THE DIRECTION OF THE PORE THAT IS ALIGNED ALONG THE EXTERNAL MAGNETIC FIELD AT 50°C 40

FIGURE 3.10: ORIENTATION OF THE MOLECULAR FRAME DEFINED BY THE G-TENSOR AND A-TENSOR AXES OF 5-DSA RADICAL WITH RESPECT TO THE REFERENCE FRAME (AXES DENOTED AS X, Y, Z) WITHIN THE LIPID BILAYER INSIDE THE AAO NANOPORES. THE ORIENTATION OF THE MOLECULAR FRAME IS DEFINED BY THREE EULER ANGLES (α , β , γ), WHICH WERE ESTIMATED BY NUMERICAL SIMULATIONS (SEE TEXT FOR DETAILS). 44

FIGURE 3.11: THE NORMALIZED SIMULATION (RED DOTTED LINE) OF DOPC MEMBRANES LABELED WITH 1 MOL% 5-DOXYL STEARIC ACID (5-DSA) ASSEMBLED WITHIN AAO FULLY DEHYDRATION AT ROOM TEMPERATURE (23OC) WHICH MEASURED BY X-BAND EPR SPECTROSCOPY (BLACK SOLID LINE) WITH DOXYL (GZZ) A) PARALLEL (BLUE SPECTRUM) AND B) PERPENDICULAR (RED SPECTRUM) TO THE DIRECTION OF THE PORE THAT IS ALIGNED ALONG THE EXTERNAL MAGNETIC FIELD. 45

FIGURE 3.12: GRAMICIDIN CHEMICAL STRUCTURE 46

FIGURE 3.13: Q-BAND (34GHZ) DEER SPECTROSCOPY OF DOPC:GRAMICIDIN A MEMBRANES IN AAO NANOPORES WITH 20% TREHALOSE. EXPERIMENTAL A) AND B) ARE DEER TRACES (BLACK LINES) MEASURED AT 76K FOR PARALLEL AND PERPENDICULAR AAO PLANE ORIENTATION WITH RESPECT TO MAGNETIC FIELD AXIS RESPECTIVELY. RED LINES ARE THE BEST FIT BY DEERANALYSYS2019 USING TIKHONOV REGULARIZATION AND ASSUMING ISOTROPIC INTER-SPIN VECTOR ORIENTATIONS IN THE SAMPLE. C) AND D) ARE THE DISTANCE DISTRIBUTIONS CORRESPONDING TO THE SIMULATED TRACES SHOWN IN A) AND B) RESPECTIVELY. 50

LIST OF TABLES

TABLE 1: PRINCIPAL G- AND A-TENSOR COMPONENTS OF 5-DSA OBTAINED FROM SPECTRUM SIMULATION.....	45
TABLE 2: ANGULAR ORIENTATION PARAMETERS (M_A , M_B , M_Γ AND Σ_A , Σ_B , Σ_Γ) OF 5-DSA IN DOPC MEMBRANES	46

1. INTRODUCTION

Biological membranes are highly dynamic supramolecular assemblies, primarily composed of lipid bilayers, that play an essential role in compartmentalization, signaling, and maintaining cellular homeostasis. The functional properties of lipid membranes arise from their fluid yet ordered structure, which is critically dependent on the presence of water. Hydration stabilizes the bilayer by supporting hydrogen bonding with lipid headgroups, mediating electrostatic interactions, and enabling the lateral mobility of lipids and proteins. Even moderate dehydration disrupts these delicate interactions, leading to lipid phase separation, loss of bilayer continuity, and in extreme cases complete collapse of the membrane structure. Such dehydration-induced destabilization compromises membrane integrity alters lipid packing, and ultimately prevents membranes from fulfilling their biological roles.

In nature, some organisms have evolved specialized mechanisms to protect their membranes against dehydration. Those include an accumulation of compatible solutes, sugars, or protective proteins. In artificial systems, however, maintaining lipid membrane structure during dehydration remains a challenge. For applications where lipid membranes are used outside of aqueous environments; for example, in biosensing, biomimetic coatings, or dry storage of membrane based on systems of strategies are needed to provide external stabilization and structural support to the bilayer.

Nanostructured materials offer a promising route to address this challenge. In particular, anodized aluminum oxide (AAO) presents a highly ordered porous architecture with tunable pore size and surface chemistry. Its well-defined nanoscale topography and mechanical rigidity make AAO an

attractive candidate for hosting and stabilizing lipid assemblies. By confining lipid membranes within or on top of AAO structures, one may reduce the extent of membrane deformation upon water loss. The nanostructured support can effectively act as a scaffold, partially replacing the role of the hydrated environment by maintaining bilayer alignment, minimizing membrane curvature stress, and preserving overall integrity during dehydration–rehydration cycles.

In this work, we investigate how AAO nanostructured substrates influence the stability and organization of lipid membranes under dehydration. Specifically, we aim to assess whether the AAO support can promote bilayer integrity and lipid alignment, thereby mitigating the structural breakdown that typically occurs under dry conditions. Our approach combines biophysical characterization methods, including electron paramagnetic resonance (EPR) spectroscopy, to probe lipid packing and dynamics, with the goal of elucidating how nanostructured supports can stabilize membrane structure in the absence of full hydration. This study contributes to a broader understanding of membrane–material interactions and may inform the design of robust membrane-based systems for biotechnological and biomedical applications.

1.1. General introduction to lipid membranes

Lipid membranes are the fundamental structural motifs of all cellular life, forming barriers that separate the inside of the cell from its external environment and enabling compartmentalization into organelles [1]. The archetypical membrane is a bilayer, typically 4 to 6 nm thick, formed through the spontaneous self-assembly of amphipathic lipids in aqueous environments [2]. Lipids are amphiphiles, composed of a hydrophilic headgroup and one or more hydrophobic acyl chains. This chemical asymmetry drives segregation into a bilayer configuration: the hydrophobic chains

face inward, away from water, while hydrophilic headgroups orient toward the aqueous exterior [3], [4].

The fluid mosaic model, first proposed by Singer and Nicolson (1972), introduced the concept of membranes as dynamic, fluid-like entities in which proteins and lipids laterally diffuse. While this model remains the conceptual foundation, modern refinements highlight the presence of nanoscale heterogeneity (lipid rafts, nanodomains), dynamic coupling to the actin cytoskeleton, and the influence of membrane curvature and tension on protein organization [2], [5], [6]. Recent high-resolution imaging and simulation studies have demonstrated that lipid bilayers are not homogeneous fluids but exhibit nanoscale ordering and fluctuating domains that contribute to biological regulation [7], [8].

Experimental structural characterization of bilayers has employed X-ray diffraction, neutron scattering, NMR spectroscopy, fluorescence microscopy, and atomic force microscopy. Such studies have established key parameters such as bilayer thickness, lipid area per molecule, and electron density profiles [9], [2], [8]. Simultaneously, molecular dynamics (MD) simulations, increasingly at atomistic resolution, now complement experiments by providing dynamic pictures of lipid-lipid and lipid-protein interactions[10]. The convergence of experimental and computational approaches has deepened understanding of how membranes maintain their fluidity while remaining structurally resilient [11].

1.2. Why lipid membrane structure is important for function

The physical properties of membranes are not merely structural; they play active roles in regulating biological processes. The hydrophobic thickness of a bilayer, for example, determines hydrophobic matching with transmembrane proteins, thereby influencing protein folding, stability, and activity

[2], [12]. Deviations in matching introduce elastic stress that can stabilize particular protein conformations or modulate activity[13], [14]. This principle explains why some membrane proteins require specific lipid environments for optimal function.

Lateral heterogeneity within bilayers further contributes to function. Lipid “rafts,” enriched in cholesterol and sphingolipids, create ordered nanodomains that act as organizing centers for signaling complexes. Although the exact nature and size of these domains remain debated, there is strong evidence that domain-driven segregation underlies receptor clustering, signal amplification, and viral budding[11], [1], [15]. Moreover, membrane curvature, influenced by lipid composition and cytoskeletal interactions, provides another dimension of structural regulation. Proteins such as BAR domains preferentially bind to curved membranes, amplifying curvature and coupling structure to trafficking pathways such as endocytosis[16].

The mechanical properties of membranes — bending rigidity (κ), area compressibility modulus (K_a), and line tension — determine how membranes respond to applied forces[2], [17]. These parameters govern processes such as vesicle fusion, exocytosis, and organelle morphology[11]. Mechanical mismatch can also trigger mechanosensitive ion channels, coupling physical deformation to electrical signals[14]. Similarly, permeability depends strongly on structural features: lipid composition, cholesterol content, and the packing of acyl chains all influence the diffusion of small molecules and ions across membranes[18].

Thus, the structure of the bilayer is inseparably linked to function, and small perturbations in lipid composition or hydration can have profound biological consequences[2].

1.3. Importance of lipid membrane hydration for stability of its structure

Hydration of lipid membranes is a central determinant of stability and dynamics. Water molecules at the lipid–water interface are not bulk-like; they exhibit restricted mobility, form hydrogen bonds with lipid headgroups, and mediate electrostatic interactions[19], [8]. This hydration layer stabilizes the bilayer by reducing headgroup repulsion and providing a structured environment that maintains spacing between adjacent membranes[20], [21].

The role of hydration becomes evident in multilamellar systems, where the spacing between bilayers is dictated by a balance of attractive (van der Waals, electrostatic) and repulsive (hydration, entropic undulation) forces. Hydration repulsion, which decays exponentially with distance, dominates at separations < 2 nm and prevents membrane collapse[20]. Experiments using osmotic stress methods and X-ray diffraction have shown that even subtle changes in hydration can alter bilayer spacing and induce phase transitions between gel, liquid-ordered, and liquid-disordered states[2], [8].

On the molecular scale, hydration directly modulates headgroup orientation and mobility. Infrared spectroscopy and NMR studies reveal that interfacial water dynamics are tightly coupled to lipid headgroup fluctuations, which in turn influence acyl chain order [22]. Reduced hydration (e.g., during dehydration stress in cells, or in experimental dry environments) destabilizes bilayers, promotes non-lamellar phases (e.g., inverted hexagonal), and impairs protein activity [23]. Conversely, adequate hydration stabilizes bilayers against thermal fluctuations and supports the functional insertion of proteins [11], [24]. The hydration-dependence of bilayer mechanics also has practical consequences for model membrane studies. Supported bilayers on solid substrates often

exhibit reduced mobility due to restricted hydration between the bilayer and support; strategies such as polymer cushions or nanostructured substrates have been developed to maintain sufficient hydration for biological relevance (Steinem et al., 1996).

1.4. Introduction to anodic aluminum oxide (AAO)

Anodic aluminum oxide (AAO) is a nanostructured material generated through the electrochemical anodization of aluminum in acidic electrolytes. Under controlled voltage and electrolyte conditions, aluminum oxidizes to form alumina with highly ordered cylindrical nanopores aligned perpendicular to the surface [25]. The diameter of pores (10–400 nm), their interpore distance, and thickness of the oxide layer can be precisely tuned by varying anodization conditions (voltage, temperature, electrolyte type) [26], [27], [28]. The self-organized nature of AAO makes it unique: long-range ordered pore arrays can be produced reproducibly over centimeter-scale areas[29].

AAO exhibits several properties attractive for biointerfacing. The material is chemically stable, mechanically robust, and optically semi-transparent in the visible range, which facilitates microscopy [30]. Its high porosity (up to 50% void fraction) and large internal surface area provide opportunities for molecular adsorption and immobilization. Importantly, the alumina surface can be functionalized using silanization, phosphonate chemistry, or deposition of secondary oxide layers to tune surface hydrophilicity, charge density, and chemical reactivity[31].

Originally explored as a template for nanowire and nanotube fabrication, AAO has since found applications in biosensing, drug delivery, and membrane biophysics. Its highly regular pore arrays provide geometric confinement at length scales commensurate with biomolecular assemblies such as lipid bilayers, making it an attractive scaffold for model membrane studies.

1.5. How AAO is used to study lipid membranes

Formation of bilayers within nanopores. AAO membranes provide vertically aligned nanopores that can be filled or coated with lipids to produce ordered bilayer arrays. Vesicle fusion and Langmuir–Blodgett/Langmuir–Schaefer transfer methods have been used to coat pore walls with bilayers, generating high-density arrays of oriented bilayers suitable for spectroscopic studies (e.g., solid-state NMR, EPR). The confined geometry enforces alignment and reduces disorder, which is advantageous for ensemble-averaging techniques [32], [33].

AAO nanopores can be coated with lipid bilayers to produce hybrid nanopores that combine the mechanical robustness of inorganic pores with the biocompatibility of lipids. Such pores reduce noise in ionic current recordings, support reconstitution of membrane proteins (e.g., α -hemolysin, ion channels), and enable biosensing of DNA or small molecules. The lipid layer also minimizes nonspecific interactions with analytes, improving the sensitivity and selectivity of nanopore devices[34].

The cylindrical geometry of AAO pores introduces curvature and confinement on the order of tens to hundreds of nanometers, enabling systematic studies of how lipid bilayers adapt to geometric constraints. These setups allow researchers to investigate curvature-induced stresses, domain formation in confined geometries, and the influence of pore size on bilayer stability. Curvature-sensitive proteins or peptides can be reconstituted in AAO-confined bilayers to probe how geometry regulates binding and activity [35].

Together, these applications make AAO a unique bridge between biological and synthetic systems, enabling the study of membranes under confinement and providing hybrid devices with potential for sensing and biotechnology.

1.6. General introduction to EPR spectroscopy

Electron paramagnetic resonance (EPR), also known as electron spin resonance (ESR), is a spectroscopic technique that detects species with unpaired electrons, such as radicals, transition-metal complexes, or spin labels. Since most biological molecules are diamagnetic, EPR is inherently selective, reporting only on paramagnetic centers. This property has made EPR, and especially site-directed spin labeling (SDSL), a central tool in modern structural biology and membrane biophysics[36], [37].

1.6.1 Basic resonance condition

An isolated electron spin ($S = 1/2$) in an external magnetic field (B_0) experiences Zeeman splitting of its spin states: $H_Z = \beta_e g B_0 S_z$

where β_e is the Bohr magneton, (g) the spectroscopic splitting factor (g -value), and S_z the spin operator along the magnetic field. The energy difference between the spin-up ($m_S = +\frac{1}{2}$) and spin-down ($m_S = -\frac{1}{2}$) states is:

The energy difference between the two spin states is: $\Delta E = h\nu = \beta_e g B_0$

where ν is the microwave frequency. At X-band frequencies ($\nu \sim 9.5 \text{ GHz}$) the resonance field for a free electron ($g = 2.0023$) is about 0.34 T [38]

1.6.2 Spin Hamiltonian

In practice, the spin Hamiltonian includes additional interactions beyond the Zeeman term:

$$H = \beta_e \cdot B_0 \cdot g \cdot S + S \cdot A \cdot I + S \cdot D \cdot S + H_{ZFS}$$

g -tensor (g): often anisotropic.

Hyperfine tensor (A): describing coupling between electron spins and nearby nuclear spins, for nitroxides, hyperfine splitting from the ^{14}N nucleus ($I = 1$) dominates.

Dipolar tensor (D): through-space coupling between two electron spins, exploited in distance measurements.

Zero-field splitting (H_{ZFS}) : relevant for high-spin systems.

For nitroxide spin labels (widely used in membrane studies), the dominant terms are the anisotropic g-tensor and the hyperfine coupling to the ^{14}N nucleus ($I = 1$):

$$H_{\text{Nitroxide}} = \beta_e \cdot B_0 \cdot g \cdot S + S \cdot A^{14\text{N}} \cdot I$$

The resulting anisotropy is partially averaged by molecular motion, producing characteristic line shapes that are highly sensitive to local dynamics [39], [40].

1.6.3 CW EPR spectral information

In continuous-wave (CW) EPR, the following observables are central:

g-values: small shifts in g reflect local electronic structure.

Hyperfine splitting: for nitroxides, the three-line spectrum reflects ^{14}N hyperfine coupling, sensitive to polarity and hydrogen bonding [41].

Line shapes and dynamics: spectral breadth and anisotropy reflect molecular motion. Rotational correlation times T_R can be extracted from simulations [39]

Order within membranes is often expressed by the order parameter (S):

$$S = \frac{1}{2}(3\cos^2\theta - 1)$$

Where θ is the angle between the probe's principal axis and the bilayer normal. High (S) corresponds to restricted orientations (gel phases, protein–lipid contacts), whereas low (S) indicates fluid environments [42].

1.6.4 Electron–electron dipolar coupling

Two electron spins separated by distance (r) interact via the dipolar Hamiltonian:

$$H_{dd} = \frac{\mu_0}{4\pi} \frac{g^2 \beta_e^2}{r^3} [S_1 \cdot S_2 - 3 (S_1 \cdot r)(S_2 \cdot r)]$$

This interaction scales as r^{-3} and encodes distance and orientation information. In CW spectra it produces line broadening, whereas in pulsed EPR (e.g., DEER) it manifests as oscillations in the time domain that can be converted to distance distributions [43].

1.6.5 CW vs Pulsed EPR

CW EPR (steady-state absorption) is powerful for probing local order, motion, and membrane phase state at ambient conditions.

Pulsed EPR (time-domain echo techniques) provides access to relaxation times and nanometer-scale distances, usually at cryogenic temperatures.

Together, CW and pulsed EPR provide a complementary toolkit for studying membrane alignment, structural integrity, and protein–lipid interactions.

1.6.6 Pulsed EPR and DEER spectroscopy

While CW EPR is invaluable for probing lipid order and motion, it lacks time-domain resolution. Pulsed EPR, introduced in the 1960s–70s, enabled coherent spin manipulation via microwave pulses [44]. The Hahn echo ($\frac{\pi}{2} - T - \Pi$) experiment is the foundation: a $\frac{\pi}{2}$ pulse creates transverse magnetization, which dephases during τ ; a π pulse refocuses spins, generating an echo at 2τ .

T1 (longitudinal relaxation): recovery of spin populations to equilibrium. Reports on spin–lattice interactions, sensitive to low-frequency motions.

T2/Tm (transverse or phase memory relaxation): decay of spin coherence. Sensitive to dipolar couplings and local field fluctuations.

In frozen biological samples, Tm is often short due to proton spin diffusion; deuteration of solvents and lipids can prolong coherence, thereby extending the DEER time window[45]

1.6.7 Distance measurements

When two unpaired electrons are within 1.5–8 nm, their dipolar interaction produces oscillations in the spin echo signal. This forms the basis for double electron–electron resonance (DEER) or pulsed electron–electron double resonance (PELDOR).

1.6.8 Four-pulse DEER

The widely used four-pulse DEER sequence was introduced by [43], enabling dead-time-free detection of dipolar couplings. One spin packet is observed, while a selective “pump” pulse inverts a partner spin at a different frequency. The resulting echo modulation encodes the distance distribution between spins.

1.6.9 Data analysis

Extracting distances from DEER data is mathematically ill-posed. The DeerAnalysis software [46] employs Tikhonov regularization and model-based approaches to recover distance distributions. Benchmarking studies [47] provide best-practice guidelines.

1.6.10 Developments

Advances include five-pulse DEER [45], high-frequency DEER (W-band, Q-band), and chirped-pulse techniques. These extend distance ranges, improve sensitivity, and make DEER increasingly applicable to membrane proteins.

EPR studies of lipid membranes: alignment and structural integrity

EPR has long been applied to lipid bilayers using either spin-labeled lipids or SDSL of membrane proteins.

1.6.11 Spin-labeled lipids

Lipids carrying nitroxides at defined chain positions (e.g., 5-, 12-, 16-DOXYL-PC) provide depth-dependent order profiles [40], [41]. CW spectra from these probes reveal:

Membrane phase: gel vs liquid-crystalline phases are easily distinguished by line shape.

Order profiles: chain order decreases from headgroup to bilayer center; cholesterol increases order particularly in the upper chain region [42].

Domain formation: multiple spectral components reveal coexisting lipid environments.

1.6.12 Protein–lipid interactions

Spin-labeled lipids also reveal annular lipids bound to proteins, distinguishable from bulk lipids [48]. Exchange rates between these pools can be inferred from temperature-dependent spectra.

Site-directed spin labeling (SDSL) of proteins

Introduced by Hubbell and colleagues [49], SDSL with nitroxides at engineered cysteines allows mapping of:

Mobility: CW line shapes indicate whether a residue is buried, flexible, or part of a rigid helix.

Accessibility: power-saturation experiments with paramagnetic quenchers (O₂, NiEDDA) provide depth profiles [50].

Distances: DEER between pairs of labels reveals conformational equilibria in channels, transporters, and oligomers [51].

1.6.13 Structural insights from EPR

Cholesterol-induced ordering and raft-like domain formation detected by DOXYL probes ([42].

Stoichiometry of annular lipids determined from deconvoluted lipid EPR spectra [48].

Conformational changes in membrane proteins mapped by DEER distance measurements (e.g., gating of ion channels, dimerization of transporters) [52].

EPR spectroscopy has proven uniquely powerful for lipid membranes, combining site-specificity, high sensitivity, and nanometer structural reach. CW EPR provides real-time information on order and alignment, while pulsed EPR/DEER yields distance constraints crucial for integrative structural biology. Combined with cryo-EM, NMR, fluorescence, and molecular dynamics, EPR

continues to illuminate how lipids and proteins maintain structural integrity and regulate function in membranes.

1.7. Lipid Membrane Stability under Dehydration and the Role of AAO Nanostructured Supports

Biological membranes are highly sensitive to hydration. The structural integrity of lipid bilayers depends critically on the presence of sufficient water molecules to stabilize headgroup interactions, maintain appropriate lateral pressure profiles, and support the dynamic organization of lipids. Upon dehydration, these stabilizing forces are disrupted: headgroup spacing collapses, hydrogen bonding networks are broken, and lipid packing becomes disordered. As a result, membranes often lose their lamellar organization, undergo phase separation, or transition into nonlamellar phases. In extreme cases, the bilayer integrity is irreversibly compromised, leading to loss of alignment and destruction of the characteristic bilayer morphology. This intrinsic fragility represents a major limitation when membranes are studied under conditions of reduced hydration or when they are incorporated into devices or biointerfaces exposed to air.

In the present work, we demonstrate that anodized aluminum oxide (AAO) nanostructured materials can serve as effective supports to preserve lipid membrane structure under dehydrating conditions. AAO provides a well-defined nanoporosity, high surface area, and mechanical rigidity, creating an environment that restricts uncontrolled lipid rearrangements. When membranes are deposited onto AAO substrates, the nanostructured topography promotes partial confinement and alignment of the bilayers, which mitigates the disruptive effects of water loss. Even under conditions of complete or partial dehydration, lipid assemblies on AAO maintain a degree of order and continuity that is typically lost in unsupported systems.

The protective effect of AAO can be interpreted as a combination of mechanical stabilization and environmental support. The rigid nanoporous framework physically constrains lipid mobility, reducing the extent of dehydration-induced bilayer collapse, while the nanoscale curvature and confinement may help preserve headgroup spacing and local hydration shells. Importantly, the interaction between lipid membranes and AAO does not prevent the bilayers from exhibiting characteristic dynamic and structural features but instead provides a stabilizing scaffold that maintains their global alignment.

Taken together, these findings indicate that AAO nanostructures are valuable tools for preserving lipid membrane integrity in challenging environments. Beyond providing insight into the fundamental biophysics of dehydration stress, this approach also highlights the potential of nanostructured supports in biointerfaces, membrane-based devices, and biophysical studies where maintaining membrane order outside of fully hydrated conditions is essential.

2. MATERIALS AND METHODS

2.1 Materials

Synthetic phospholipid DOPC, DPPC, Gramicidin A and spin labeled doxyl steric acid 5 (5-DOXYL Stearic acid) were purchased from Avanti Polar Lipids in chloroform solutions; Gramicidin from *Bacillus brevis* was purchased from Fischer Scientific Co. LLC (Pittsburgh, PA), as a mixture of gramicidin A, B, and C; D-(+)-Trehalose (TCI, Tokyo Chemical Industry Co., Ltd., Product No. T0832, > 98 % GC); Ficoll® 400 (Sigma-Aldrich, Merck KGaA, Darmstadt, Germany; Cat. No. F4375); AAO membranes (Whatman, Ltd., Middlesex, U.K.), 60 µm thick, with a pore diameter of 200nm.

2.2 Sample preparation

Multilamellar vesicles (MLVs): Spin-labeled multilamellar vesicles were prepared by mixing chloroform solutions of DOPC or DPPC with 5DSA in 100:1 molar ratio. The mixture of lipid and 5DSA was dried under nitrogen gas, leaving a thin film of lipid deposited on the bottom of the vials. Residual chloroform was removed by keeping the vials on a vacuum pump overnight. The lipids were resuspended in the buffer by adding 50mM HEPES, pH 7.0, buffer to the final lipid concentration of 20 vol% in the mixture and vortex extensively. After that the sample was incubated 40 min in a water bath at $T_m=25^\circ\text{C}$ for DOPC and $T_m=50^\circ\text{C}$ for DPPC before forming MLVs by cycling flask for at least 10 times between liquid nitrogen (77K) and water bath at 298 K for DOPC and 323K for DPPC. The vials were stored at 5oC for further use.

Gramicidin A spin-labeling procedure: Gramicidin A (250 mg) was dissolved in 5 mL of ethanol, concentrated under reduced pressure, and dried overnight under high vacuum in a reaction flask. Anhydrous GA was dissolved in 3.5 mL of anhydrous dimethylformamide (DMF) and 37.24 mg of 2,2,5,5-tetramethyl-3-pyrrolin-1-oxyl-3-carboxylic acid (TPC), 41.27 mg of dicyclohexylcarbodiimide (DCC), and 2.81 mg of 4-dimethylaminopyridine (DMAP) were added. The reaction mixture was stirred at room temperature for 48 h.

The reaction mixture was diluted with 5.5 mL of water to induce precipitation. The precipitate was collected on a sintered glass filter and dried under vacuum. The crude material was dissolved in 1.5 mL of chloroform/methanol (90:10, v/v) and analyzed by thin-layer chromatography in the same solvent system. TLC analysis showed two major bands, one band with $R_f=2.7\text{cm}$ corresponding to a small amount of unreacted GA and another, significantly larger band with $R_f=5.7\text{ cm}$ corresponding to less polar component of the reaction mixture and consistent with formation of the spin-labeled GA (Figure 2.1).

The product was purified by chromatography on a preparative TLC plate (silica gel 60 F₂₅₄, 1mm) eluting with mixture chloroform/methanol (90:10, v/v)[53].



Figure 2.1: Comparison under UV illumination of GA spin-labeled(right) $R_f = 5.7$ cm and GA control (left) with $R_f = 2.7$ cm in thin-layer chromatography.

2.3 Preparation of AAO Nanopores Samples with DOPC (MLVs) or DPPC (MLVs)

DOPC Loading: A measured volume of the mixture (DOPC:5DSA) with ratio (100:1) solution was carefully applied onto the AAO surface using a calibrated micropipette. The sample was then left to dry at ambient laboratory conditions (23°C, typically 50-60% relative humidity) to promote bilayer formation within the nanopores. After sufficient drying, surplus lipid not incorporated within the pores was gently removed from the AAO surface using a Q-tip, ensuring that the remaining lipid was primarily confined inside the nanopores.

DPPC Loading: For the incorporation of DPPC, the mixture (DPPC:5DSA) with ratio (100:1) solution was applied onto the AAO surface in a similar fashion using a micropipette. To facilitate effective penetration and distribution of DPPC into the nanoporous structure, the sample was

gently heated on a hot plate set at 50°C. Once the lipid film had adhered and excess water had evaporated, the surface was carefully wiped with a Q-tip to eliminate any DPPC remaining on the external surface, thereby maximizing lipid localization within the pores.

DOPC and Gramicidin A–Labeled Loading: A DOPC/Gramicidin A-labeled solution (100:1 molar ratio) was applied to the surface of anodic aluminum oxide (AAO) membranes using a calibrated micropipette. Samples were dried under ambient laboratory conditions (23°C, 50–60% relative humidity) to facilitate bilayer formation within the nanopores. Following drying, excess lipid not incorporated into the pores was carefully removed from the membrane surface with a cotton applicator, leaving the lipid primarily confined within the nanoporous structure.

Preparation of Trehalose-Modified Samples: Aqueous trehalose solution (20% w/v) was freshly prepared for use with lipid-loaded AAO membranes. For each sample, 20 µL of the trehalose solution was applied directly onto the AAO membrane that had previously been loaded with either DOPC, DPPC and DOPC:Gramicidin A. Samples were subsequently allowed to dry at room temperature (23°C, 50–60% relative humidity), enabling trehalose to interact with the confined bilayer structures. This step supports the study of the protective effects of trehalose under nanoconfined and dehydrating conditions.

2.4 Preparation of samples at different hydration Levels

The sample was exposed to different levels of relative humidity (RH%) after drying off extra water. To create a controlled humidity environment, nitrogen gas with a specific RH was flowed over the sample using a setup built at NCSU (Figure 2.1A). The system used three flow meters, manual valves, a water container, and an electronic hygrometer that can measure humidity from 10% to 95%. The nitrogen's humidity was controlled by mixing wet nitrogen gas (about 90% RH) and dry

nitrogen gas (about 10% RH). The final RH and temperature of the nitrogen gas reaching the sample were constantly checked with the hygrometer.

When studying lipid bilayers under various humidities, the sample could be exposed immediately to wet nitrogen at 90% RH. For other RH values, the sample was placed inside the EPR cavity (Figure 2.1B) and allowed to adjust to the humidity for about 10 min before measurements started. Humidity gradually decreased from 95% to 75%, then 50%, 25%, and finally dry nitrogen at 10% RH was used during EPR experiments. If needed, dried samples were rehydrated by flowing wet nitrogen and increasing RH.

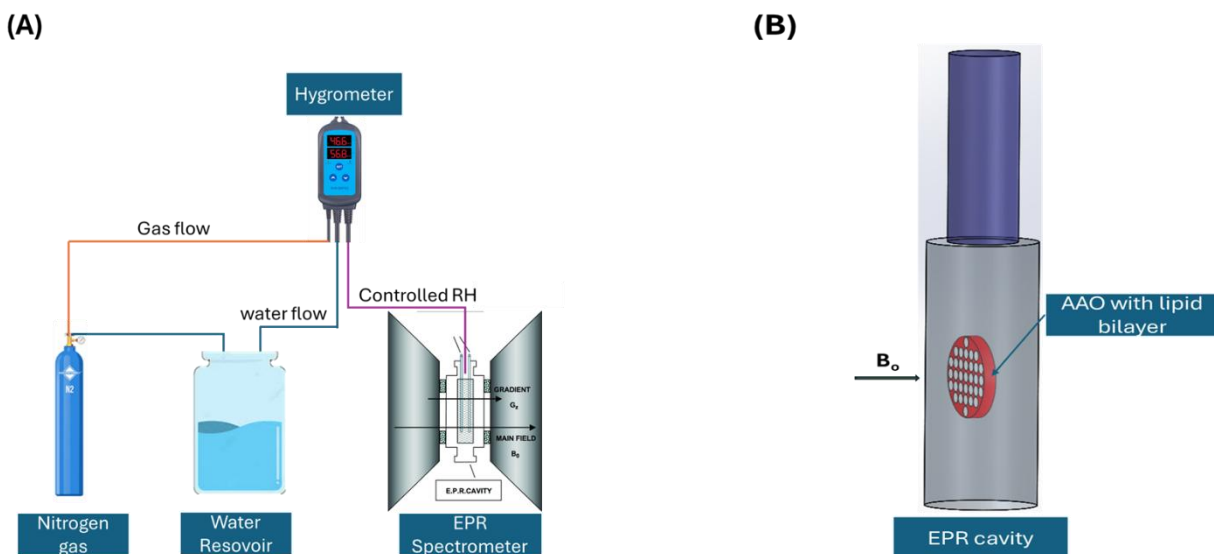


Figure 2.2 (A) Schematic representation of NCSU-built humidity-controlling setup for a sample inside EPR cavity. (B) Samples AAO with lipid bilayer inside EPR cavity with AAO surface perpendicular to the polarizing magnetic field.

2.5 Variable Temperature Experiments

Sample temperature was controlled by a Variable temperature accessory based on the Polyscience 8002A11B Digital Temperature Controller provides precise temperature regulation for laboratory use, high stability (as $\pm 0.05^{\circ}\text{C}$)

2.6 X-band CW-EPR measurements

X-band (9.5 GHz) EPR measurements were carried out with a Varian Century Series E-102 spectrometer (Palo Alto, CA) which was interfaced with a personal computer. All spectra were digitized to 2048 data points. Typical spectrometer settings were as follows: incident microwave power: 20 dB; sweep time: 30 s; modulation amplitude: 0.2 G; scan width: 160 G; center field: 3385G.

2.7 Pulsed Q-band (34GHz): DEER spectroscopy

A Bruker ELEXSYS E580 spectrometer equipped with SuperQFTu bridge, 10 W AmpQ amplifier, and Q-band EN 5107D2 dielectric resonator (Bruker Biospin, Billerica, MA, USA) has been employed for all experiments. Dehydration sample (DOPC:Gramicidin A with trehalose embedded AAO) were loaded into Suprasil WG-222T tubes (o.d. = 1.6 mm, i.d. = 1.1 mm; Wilmad LabGlass, Vineland, NJ, USA), sealed at one end, flash-frozen in liquid nitrogen, and rapidly transferred into a pre-cooled Q-band resonator. The experiment were conducted at 76 K using a Bruker ER4118CF flow cryostat cooled with liquid nitrogen. No cryoprotectant was employed.

For DEER measurements, the pump frequency was set 60 MHz higher than the observer frequency, with the magnetic field adjusted to pump spins at the maximum of the nitroxide spectrum. Observer $\pi/2$ - and π -pulses were 12 ns and 20 ns in length, respectively, and the pump π -pulse length was 22 ns. The interval between the first and second observer pulses (τ) was 160 ns, and the delay

between the second observer pulse and the onset of the pump pulse was 60 ns. Each dipolar evolution point was acquired with 200 shots per scan, using a shot repetition time of 1 ms. All spectra were collected with standard 8-step phase cycling.

2.8 Software Computer

Simulations of EPR spectra of spin-labeled lipid bilayers were carried out using EasySpin, MatLab, and DEERAnalysis2019.

3. RESULTS

3.1 X-band EPR Characterization of Hydrated 5-DSA-Labeled DPPC Membranes Aligned Inside AAO Nanopores (Temperature= 23°C)

We studied the effect of temperature on the EPR spectra of the DPPC membranes doped with 1 mol% 5-DSA by CW X-band EPR spectroscopy. Typical EPR spectra are shown in Figure 3.1; The spectrum collected at 25°C (black line) revealed broad lines that are indicative of the limited motional freedom caused by tightly packed acyl chain of DPPC lipid in gel phase. At a higher temperature, 35°C (red spectrum) the spectrum is essentially the same as that measured at 25°C with $A_{zz} = 30.728\text{G} \pm 0.03$ because DPPC bilayer is still in gel phase. At 45°C (blue) the spectrum exhibits slightly lower $A_{zz} = 25.5005\text{G} \pm 0.03$ value indicating that in liquid-crystalline phase ($T_m=41^\circ\text{C}$) the acyl chains of DPPC molecules became more flexible and less ordered, causing some averaging of g- and A anisotropic. Overall, the observed changes in the spectral features are consistent with the temperature induced changes in structural dynamics of DPPC bilayers observed using EPR spectroscopy and reported in the literature [54].

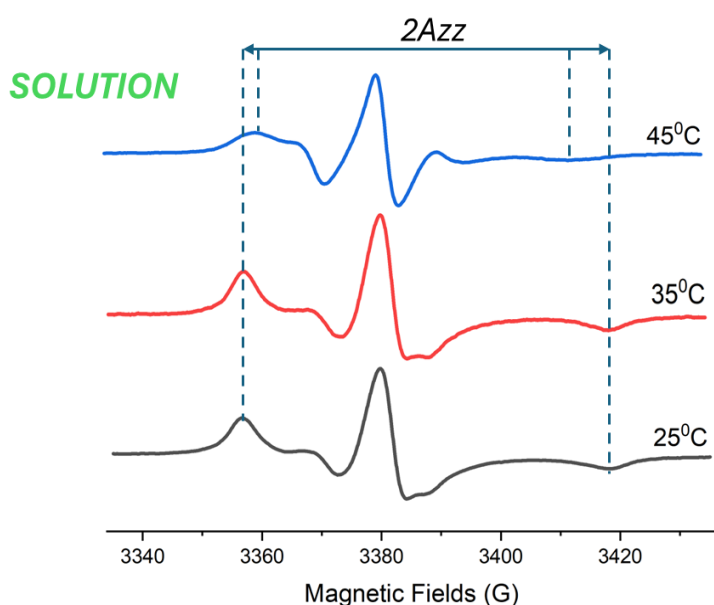


Figure 3.1 Temperature-dependent EPR spectra of aqueous suspensions of DPPC MLVs doped with 1 mol% 5-doxyl stearic acid (5-DSA) in buffer solution (50mM HEPES, pH 7.0) at 25 °C, 35 °C, 45 °C.

The EPR spectra of AAO nano template loaded with DPPC:5DSA sample as described above and maintained hydrated were measured to investigate the influence of nanoconfinement on the mobility of lipids and bilayer organization. The spectra shown in Figure 3.2 are significantly different compared to the spectra from DPPC:5DSA sample in the solution (Figure 3.1). For the hydrated DPPC sample (Figure 3.3, blue spectrum), when the external magnetic field is parallel to the AAO plane (Figure 3.3 blue trace), the EPR spectrum is broader compared to the one obtained from the AAO plane oriented perpendicular to magnetic field (red spectrum). As we can see, the spectral features corresponding to A_{zz} spectral component are essentially missing in this spectrum obtained from sample with perpendicularly oriented AAO plane. The main reason for an essential disappearance/suppression of A_{zz} component is the macroscopic alignment of the phospholipids when confined in AAO. In nitroxides nitrogen hyperfine and g -tensors are approximately collinear i.e. their principal axes have nearly identical orientations. For 5-membered ring nitroxides, g_{xx} (as well as A_{xx}) lies along the direction of N-O bond, g_{yy} (A_{yy}) is oriented perpendicular to the N-O group, but lies in the ring-plane and g_{zz} (A_{zz}) is perpendicular to both the direction of the N-O bond and the ring-plane (Figure 3.2B). For the spin-doped DPPC lipid with 5-doxyl steric acid (Figure 3.2A) at the position 5th carbon atom of the chain (Figure 3.2C), the 5-membered ring plane of the radical is oriented in a way that the vector normal to the plane is parallel to the direction of the lipid alkyl chain. Thus, the DSA magnetic z -axis (g -tensor as well as hyperfine tensors) is along the lipid alkyl chain direction as shown in the figure 3.2D. When DPPC lipids doped with 5DSA were arranged inside AAO (Figure 3.2E) the magnetic z -axis remains always to be approximately parallel to the AAO plane. Therefore, if AAO is set perpendicular to the external static magnetic field direction, for every lipid orientation inside the AAO nanopores, their

corresponding magnetic z-axes remain roughly perpendicular to the direction of the field. This in turn results in disappearance (or suppression) of the hyperfine z-components from the measured EPR spectra.

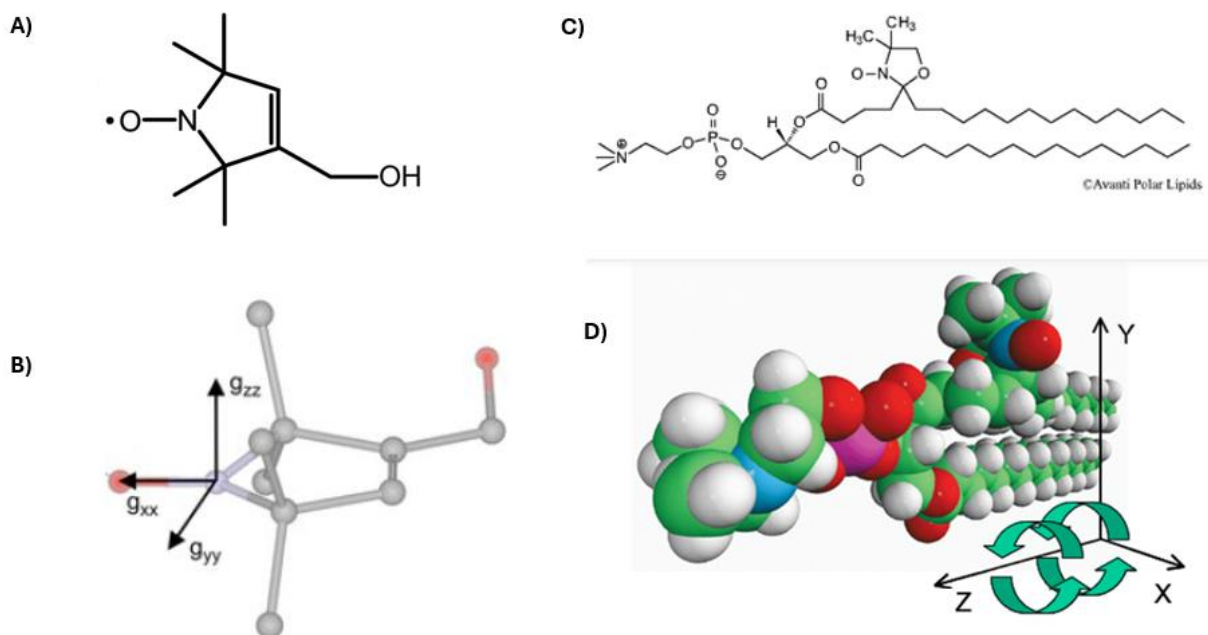
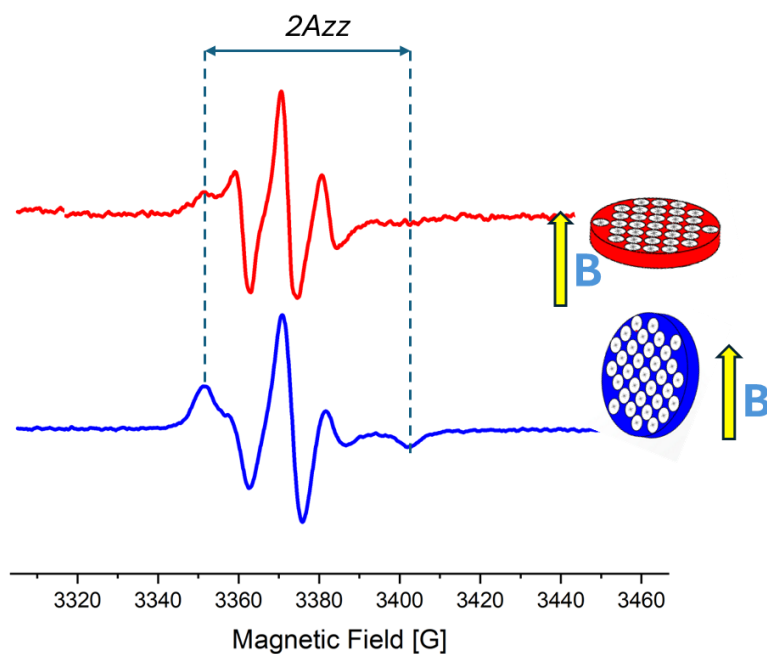


Figure 3.2: A) Chemical structure of Tempol (4-hydroxy-2,2,6,6-tetramethylpiperidine-1-oxyl) nitroxide. B) Nitroxide at 3D view with three dimensions including g_{xx} , g_{yy} and g_{zz} . C) Chemical structure of 16:0-5 Doxyl PC ((1-palmitoyl-2-stearoyl-(5-doxyl)-sn-glycero-3-phosphocholine) lipid containing DOXYL nitroxide at the position 5th of acyl chain in 2D. D) 16:0-5 Doxyl PC in 3D. E) DPPC:5DSA are self-assembling inside AAO into cylindrical structure with DOXYL z-magnetic axis (g_{zz}) perpendicular to the direction of the pore that is aligned along the external magnetic field.

Thus, the suppression of the hyperfine features due to A_{zz} tensor component for the sample where AAO plane was oriented perpendicular to the field axis as compared to that of parallel orientation (Figure 3.3) provides strong evidence of the lipids to be well-oriented inside AAO nanopores. Of great importance is that the hyperfine features observed in both spectra (field being parallel and thus perpendicular to AAO plane) correspond to moderately mobile radicals, indicating that the membrane remains partially fluid despite the confinement.



*Figure 3.3 EPR (X-band) spectra of DPPC membranes labeled with 1 mol% 5-doxyl stearic acid (5-DSA) inside AAO are self-assembling with hydration conditions including magnetic axis with DOXYL (g_{zz}) parallel (**blue spectrum**) and perpendicular (**red spectrum**) to the direction of the pore that is aligned along the external magnetic field.*

3.2 EPR Characterization of 5-DSA-Doped DPPC Membranes Embedded in AAO with/without Ficoll under Dehydration at (Temperature = 23°C)

After measuring the sample hydrated with buffer solution inside AAO, we measured room temperature EPR spectrum of the same sample but after them being slowly dried (Figure 3.4A). The spectrum has highly pronounced features due to Azz hyperfine component and more importantly is highly similar to those known (reported) for randomly oriented nitroxes (powder samples) [55], [56]. This clearly indicates a complete loss of the lipid alignment inside the AAO nanopores under the fully dehydrated condition. By other words, inside the AAO nanopores,

In an attempt to preserve at least partially the lipid membrane structure as well as lipid orientation selectivity, we made and measured a fully dried sample but this time with Ficoll sugar added. Large molecular size of Ficoll and its highly hydrophilic nature prevents its penetration inside the lipid membrane leading to the replacement of water around the lipids by this sugar. This leads to protection of the membrane structure, which is generally used to stabilize biological systems under stress during freezing [57], [58]. As a result, dried AAO DPPC samples were exposed to 20% vol aqueous solution of Ficoll and later dried again to remove the remaining water. The corresponding spectrum is shown in the Figure 3.4B. As can be seen from the figure, the spectrum is nearly identical to that obtained earlier for the dried sample but not containing any sugar. As discussed above, the spectrum is very similar to those known powder samples of nitroxides indicating absence of any preferred orientation of the radicals. Thus, we can conclude that addition of Ficoll does not promote collective alignment of the dehydrated lipids inside the AAO nanopores.

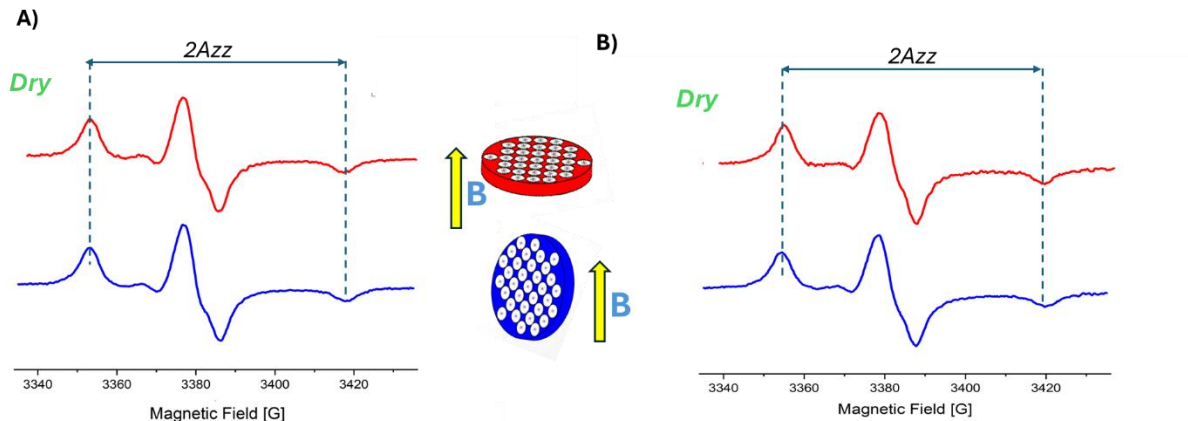


Figure 3.4 X-band EPR spectra of DPPC membranes containing 1 mol% 5-doxyl stearic acid (5DSA) spin labels confined in anodic aluminum oxide (AAO) nanopores inside AAO are self-assembling with dehydration conditions at room temperature (23°C) including magnetic axis with DOXYL (g_{zz}) **parallel (blue spectrum)** and **perpendicular (red spectrum)** to the direction of the pore that is aligned along the external magnetic field with (A) without (B) with Ficoll.

3.3 EPR Characterization of 5-DSA-Doped DPPC Membranes Embedded in AAO with Trehalose under Dehydration at (Temperature = 23°C)

Large molecular size sugar, Ficoll, was used in an attempt to prevent lipid aggregation and preserve at least partially alignment of DPPC lipids inside AAO nanopores for fully dehydrated samples. However, as discussed above, this approach failed with no observable effect on lipid orientation selectivity. As a possible reason for failure, we considered the extreme molecular size of the Ficoll sugar. Thus, a sugar with a smaller molecular size could be more suitable for the goal of preservation of the membrane structure under dehydrated condition. Trehalose is a sugar of smaller molecular size than Ficoll but still should be functionally very similar to Ficoll in terms of substituting water in the dehydrated samples [59], [60]. Indeed, similarly to Ficoll, Trehalose forms

hydrogen bonds with lipid and protein headgroups, which is expected to help to stabilize the lipid membrane structure and to preserve bilayer membrane fluidity after dehydration.

The EPR spectrum obtained at room temperature (23°C) for the sample fully dehydrated after addition of 20% vol aqueous solution of Trehalose is shown in Fig. 3.5A. In contrast to the earlier discussed data for the case of no sugar and Ficoll containing sample, the two spectra obtained for magnetic field parallel and perpendicular to AAO plane exhibit significant differences. The most pronounced difference is that spectral features caused by A_{zz} hyperfine components are significantly suppressed for the sample with the perpendicular orientation. This clearly indicates the non-randomness of the lipid orientations with the preference of the molecular magnetic z-axis to be along the direction perpendicular to the pore surface i.e. along the direction of the DPPC alkyl chains. This provides a strong evidence of Trehalose playing a significant role in protecting the lipid membrane integrity and thus in enhancing membrane structure stabilization during dehydration. Thus, we suggest, that strong H-bonding interaction of Trehalose with lipid headgroups promotes the integrity of the bilayer and helps to preserve its spatially anisotropic structure inside the nanopores.

In order to test if the membrane integrity induced by the addition of Trehalose is preserved above gel-liquid phase transition of the DPPC lipids, we performed additional measurements of EPR spectra of the same sample but at 50°C (phase transition temperature is 41°C). The corresponding spectra for both parallel and perpendicular orientations of the AAO plane with respect to magnetic field are shown in the Figure 3.5B. The spectra including the significant differences for the two orientations are very similar to those obtained at 23°C, except the somewhat more narrow (respectively more intense) spectral features observed at higher temperature. While as expected, this narrowing of the spectral features indicates a greater rotational mobility of the lipids, the

remaining spectral differences for two AAO orientations indicate the preservation of the partial alignment above the phase transition.

As a short summary of experimental observations, we can conclude that in contrast to large molecular size Ficoll, Trehalose promotes the membrane integrity as well as partial alignment of the lipids (DPPC in this particular case) in AAO nanopores in the dry condition both below and even above the gel-liquid phase transition when molecular disorder is stimulated by enhanced lipid mobility.

The main protective effect to the membrane integrity and alignment comes mainly from direct hydrogen bonding with the membrane head groups. However, Trehalose does not bind to the lipid headgroups as tightly as native water. Thus, there can still be a slight loss of membrane integrity and alignment order as compared to when the membrane is fully hydrated. As a result, while trehalose “freezes” the headgroup dynamics and adds some stability, but it cannot fully replicate the fluidity and flexibility that water provides in a hydrated bilayer. [61], [62]

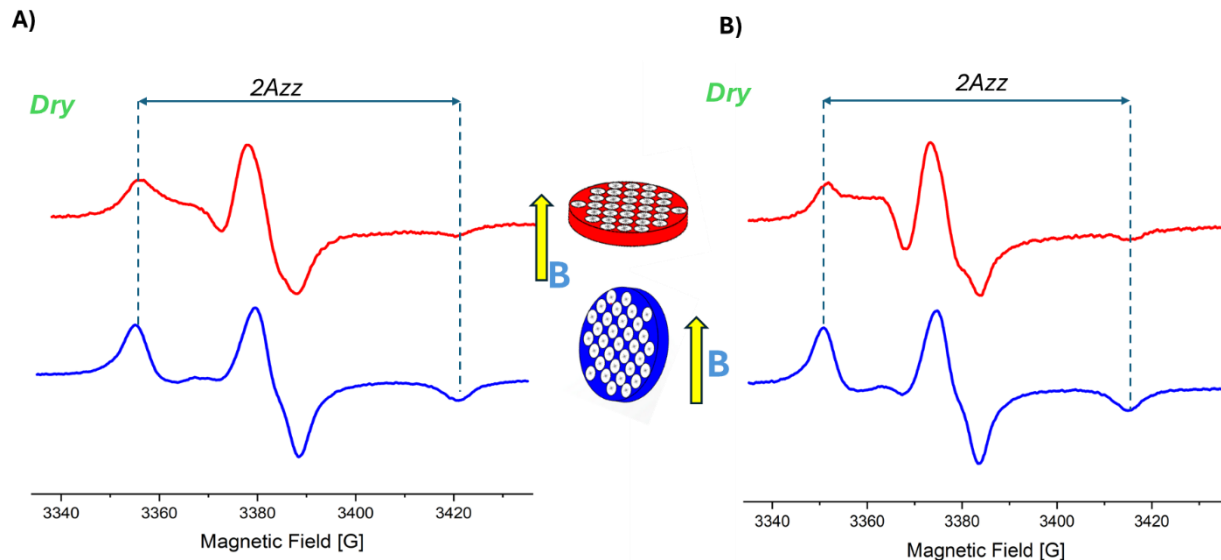


Figure 3.5 EPR (X-band) spectra of DPPC membranes labeled with 1 mol% 5-doxyl stearic acid (5-DSA) inside AAO are self-assembling with 20% vol Trehalose solution under dehydration conditions including magnetic axis with DOXYL (gzz) parallel (**blue spectrum**) and **perpendicular (red spectrum)** to the direction of the pore that is aligned along the external magnetic field at (A) 23°C, (B) 50°C

3.4 Humidity control inside AAO

3.4.1 Humidity-Dependent Behavior of 5-DSA-Labeled DPPC Membranes within AAO under Dehydration at 23 °C

As shown in the previous sections, the structural integrity of the DPPC membranes at least partially can be restored in two different ways: either by rehydration of the dried lipids or by adding a sugar of a smaller molecular size (Trehalose in our case, discussed above) to samples and drying them afterwards. To obtain more details on how rehydration affects and restores the membrane integrity and alignment, we performed a series of EPR measurements on orientation of DPPC lipids doped with 5-DSA inside the AAO nanopores (in the absence of sugar) under controlled humidity conditions and at room temperature of 23°C. For this purpose, we used wide range of humidity

levels: 10%, 25%, 50%, 75% and 95%. The first EPR measurement was done after drying the sample outside the EPR cavity and transferring the sample into the cavity where the humidity level was measured to be 10% without adding additional moisture to the air. sample test was to leave dry outside at the room temperature before putting inside cavity which sets up the humidity around 10% (at 23°C). Then the EPR spectra were measured while humidity level gradually rose from the lowest 10% to the highest 95%. To test the reversibility of the observed changes the humidity level was then gradually reduced back to its lowest value of 10%. All the measured spectra were found to be independent of the previous level of humidity level with all spectral changes to be well reproduced in the reversibility test measurements.

Even though the results are shown in Figure 3.4, we aim to further investigate the dryness of our sample in the absence of trehalose. Overall, the value of $2A_z$, which indicates hyperfine lines as a function of humidity, shows a maximum distance at 10% humidity and becomes narrower as humidity increases. This also tells us about the rising membrane fluidity and enhanced rotational freedom of the spin probe due to water content.

The EPR spectra measured for two principal AAO plane orientations (AAO plane parallel and perpendicular to the magnetic field direction) at 23°C and different humidity levels are shown in Figure 3.6. The membranes integrity was monitored by comparison of the intensities of the hyperfine features due to A_{zz} splitting for two AAO orientations. As discussed in the previous sections, the lower intensity of the A_{zz} features for perpendicular AAO orientation (Fig 3.6B) as compared to parallel AAO orientation (Fig 3.6A) provides direct evidence of membrane alignment inside AAO nanopores. By carefully inspecting data shown in Fig. 3.6, we can draw the following conclusions. At low humidity levels the A_{zz} features for two orientations are nearly indistinguishable, indicating absence of any observable lipid alignment inside the AAO nanopores.

While humidity level rises, the slow decrease of the Azz features starting from ca 50% humidity level become gradually more observable for the perpendicular AAO plane orientation indicating slowly increasing DPPC lipid alignment and thus the membrane integrity. It is very interesting and important to note that even at 95% humidity level the degree of alignment as well as overall mobility of the 5-DSA doped DPPC lipids is significantly lower than those observed for fully rehydrated samples (see section 3.1). Thus, while it is not a part of the study presented here, a more detailed study of the DPPC lipid alignment for very high humidity levels (above 95%) is of great interest and will be carried out in the near future. Nevertheless, the results shown here provide a deeper understanding of the importance of humidity in maintaining the lipid membrane structural integrity as well as the reversibility of the process upon drying/humidifying the membrane. Another interesting conclusion is that the restoration of the lipid alignments (at least for DPPC) starts at rather high humidity levels and is not complete even at humidity level of 95%.

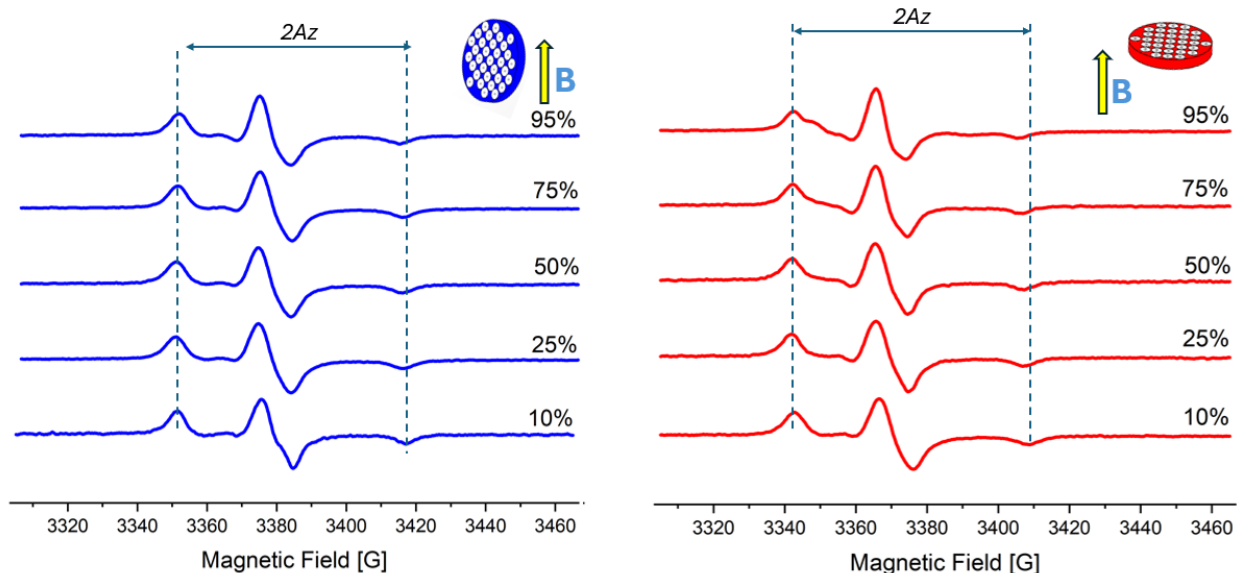


Figure 3.6: EPR (X-band) spectra of **DPPC** membranes labeled with 1 mol% 5-doxyl stearic acid (5-DSA) inside AAO are self-assembling with a range of relative humidity conditions (10-95% RH) at 23°C inside EPR cavity including magnetic axis with DOXYL (g_{zz}) parallel (**blue spectrum**) and perpendicular (**red spectrum**) to the direction of the pore that is aligned along the external magnetic field.

3.4.2 Humidity-Dependent Behavior of 5-DSA-Labeled DOPC Membranes within AAO under Dehydration at 23°C

Effect of the lipid structure on membrane integrity

As shown and discussed above, both high humidity levels and/or presence of sugars of a smaller molecular size play crucial role for the restoration/preservation of membrane integrity of the fully dehydrated lipids. The next important question rises: does the structure of the lipids composing the membrane play any significant role in maintaining the membrane integrity under the dehydration process. For this purpose, we performed a series of EPR measurements analogous to those described above for DPPC lipids, but this time for DOPC lipids. Both DPPC and DOPC are

structurally similar except for two important differences: 1) the length of alkyl chains is different (DPPC has 16 carbon atoms and DOPC has 18 carbon atoms) and 2) the presence of saturation for the DPPC lipid vs unsaturated alkyl chain for DOPC. These structural differences are the cause of differences in biophysical properties of the membranes composed of either of these two lipids. First, in membrane DPPC molecules are packed more tightly together. This is because the absence of double bond results in higher flexibility of the alkyl chain and thus steric access to more tight conformations. Second, the gel to liquid phase transition temperatures of these two lipids differs significantly: phase transition of DPPC and DOPC are at 41°C and – 17°C respectively. Thus, at room temperature (23°C) lipid bilayers of these two lipids are in two different phases: DOPC is in fluid phase and DPPC is in more rigid and ordered gel phase. As discussed above, if there is no sugar added at room temperature, the fully dehydrated DPPC bilayer loses (reversibly) its structural integrity. An important question arises whether the loss of structural integrity is related in any way to the chemical structure and/or to the phase of the lipids composing the membrane. In the following the results of three sets of EPR experiments are described in detail: 1) DOPC lipids deposited inside the AAO nanopores under controlled humidity condition in the absence and 2) in the presence of small molecular size sugar Trahalose as well as 3) fully dehydrated DPPC lipids deposited inside the AAO nanopores at 50°C in the absence of sugar.

3.4.3 DOPC: controlled humidity and no sugar added.

The series of EPR spectra obtained for DOPC lipid bilayer doped with 5-DSA under the wide range of humidity levels (from 10% to 94 %) for two principal orientations of AAO plane are shown in the Figure 3.7. It is very interesting to note that in contrast to DPPC, even for fully dehydrated membranes (humidity level 10%) the spectra corresponding to two principal AAO orientations exhibit significant well pronounced differences. The most important of them is the

significant suppression of the hyperfine features due to Azz hyperfine splitting for the AAO plane orientation perpendicular to the magnetic field direction. As described in previous sections, this provides direct evidence for the partial alignment of the lipids inside the membrane bilayer and thus partial preservation of membrane integrity.

As humidity level increases, the described spectral differences (mainly suppression of the Azz features for perpendicular AAO orientation) get gradually more pronounced. For the highest measured relative humidity level of 94%, nearly complete suppression of the hyperfine Azz features is observed for the spectrum corresponding to perpendicular AAO plane orientation. At the same time the observed changes for these Azz hyperfine features for the parallel AAO plane orientation were found to be subtle for the entire range of humidity levels. Another, although lesser pronounced spectral changes induced by the increase of relative humidity level are the visible narrowing of all spectral features for both AAO plane orientations. This observation can be explained by increase of the mobility of the 5-DSA doped lipids for higher hydration levels of the lipid membrane.

In short summary, the observed changes in EPR spectra with increasing relative humidity level demonstrate water's critical role in enhancing lateral diffusion and more importantly dynamic ordering of DOPC bilayers under nanoconfinement at room temperature. EPR data show a continuous crossover from a more restricted to a highly mobile and aligned membrane state induced by the increasing humidity of the DOPC membranes and emphasize the paramount role of hydration in membrane dynamics and structural organization in AAO templates.

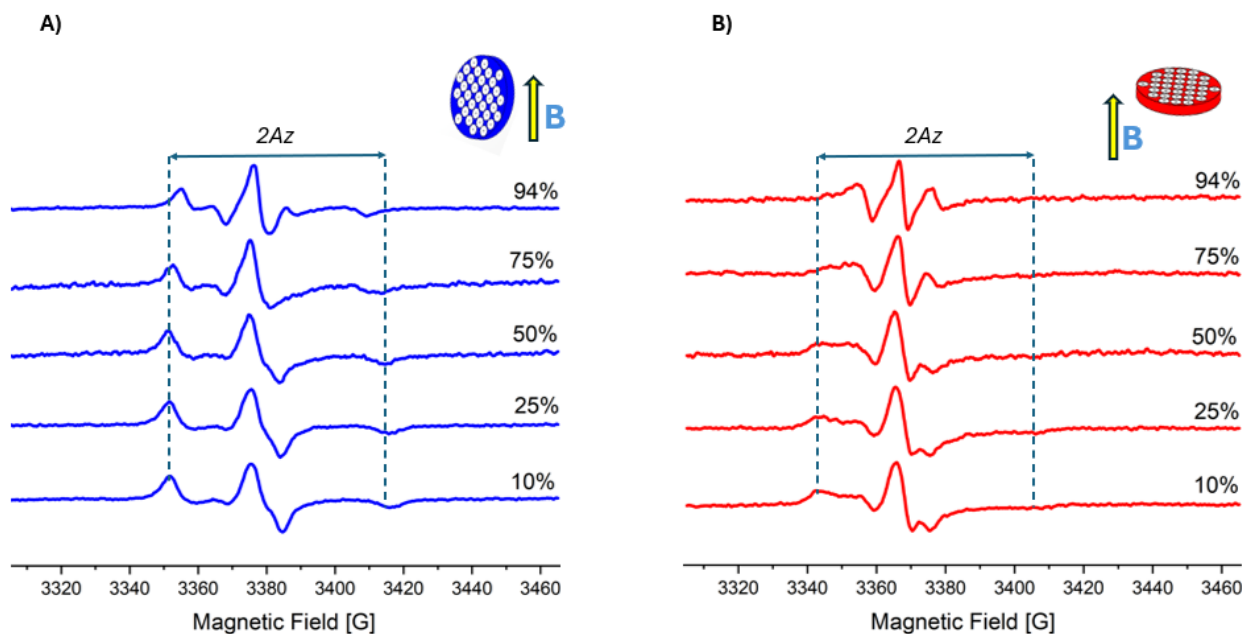


Figure 3.7 EPR (X-band) spectra of **DOPC** membranes labeled with 1 mol% 5-doxyl stearic acid (5-DSA) inside AAO are self-assembling with a range of relative humidity conditions (10-95% RH) at 23°C inside EPR cavity including magnetic axis with DOXYL (g_{zz}) parallel (**blue spectrum**) and perpendicular (**red spectrum**) to the direction of the pore that is aligned along the external magnetic field..

3.4.4 DOPC: controlled humidity and Trehalose added.

As discussed above, the presence of small molecular size sugars promoted partial alignment of the DPPC:5-DSA lipids being in gel phase at room temperature even for fully dehydrated lipids. An interesting question arises whether presence of Trehalose can further enhance the membrane integrity for DOPC lipids which are in fluid phase at room temperature and importantly partially preserve their alignment in fully dehydrated phase.

The series of EPR spectra measured for DOPC:5-DSA lipids in presence of Trehalose for wide range of controlled relative humidity levels (from 10% to 94%) are shown the Figure 3.8A for

parallel AAO plane orientation (with respect to magnetic field axis) and in Figure 3.8B for perpendicular AAO orientation respectively. Overall, the observed spectra are similar to those measured earlier in the absence of sugar (Fig. 3.7).

Similarly to the case when Trehalose was absent in the samples, overall increase of the lipid mobility is observed upon increase of the relative humidity level.

However, the observed lipid alignment judged by the suppression of the A_{zz} hyperfine features for perpendicular AAO orientation was not further improved upon adding the sugar. On the contrary, small but clearly observable decrease of the degree of the lipid alignment can be seen from the comparison of the two EPR spectra series for the entire range of relative humidity levels (with and without sugar). This is somewhat surprising as for DPPC:5-DSA lipids, trehalose has been shown to enhance lipid alignment and help maintain membrane integrity (see section 3.4). As discussed above the main protective effect of adding Trehalose was suggested to be due to binding of Trehalose to membrane surface. However, the protective effect is weakened by Trehalose penetrating to the membrane middle separating the two lipid layers. If Trehalose is added prior to humidifying the membrane, the sugar molecules might prevent effective penetration and binding of external water via either steric hindering and/or competitive binding to the membrane head groups.

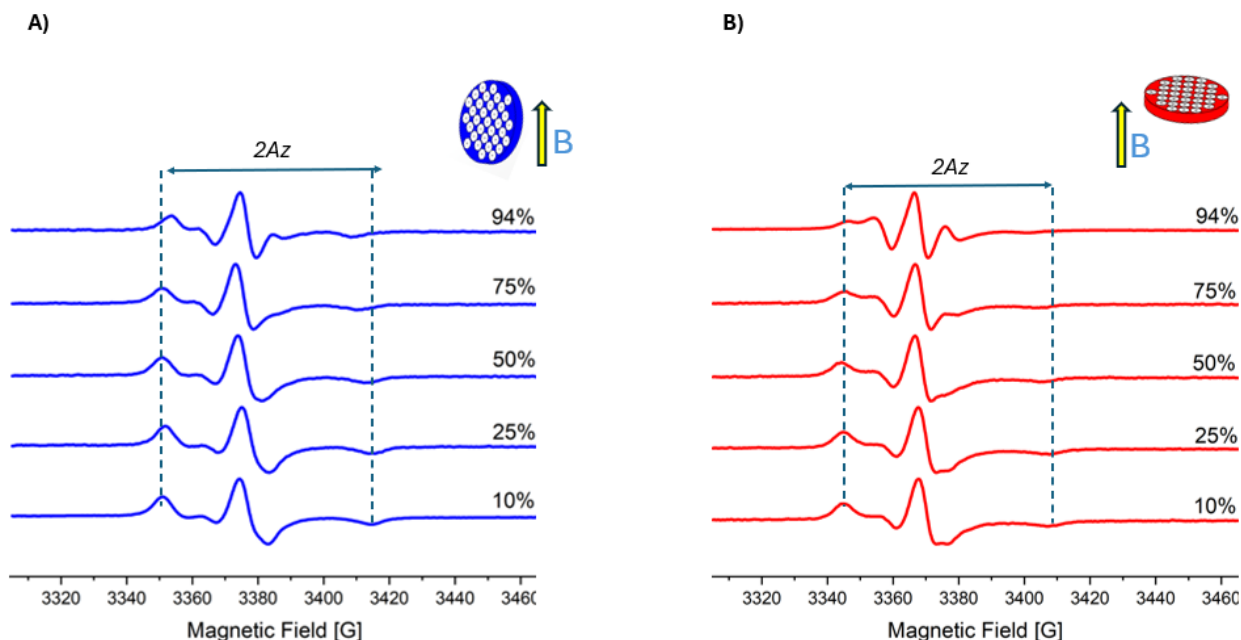


Figure 3.8 EPR (X-band) spectra of **DOPC** membranes labeled with 1 mol% 5-doxyl stearic acid (5-DSA) assembled within AAO and stabilized with trehalose 20% (w/v) solution. The spectrum was measured under a range of relative humidity conditions (10-95% RH) at 23°C inside EPR cavity including magnetic axis with DOXYL (g_{zz}) parallel (**blue spectrum**) and perpendicular (**red spectrum**) to the direction of the pore that is aligned along the external magnetic field.

3.4.5 DPPC:5-DSA doped inside AAO nanopores at 50°C

This far we have observed that preservation of membrane integrity and alignment order inside AAO nanopores upon dehydration was highly dependent on the membrane lipid composition. It was found that for membranes composed of DOPC lipids, the effect of dehydration on the alignment loss at room temperature was much smaller as compared to DPPC lipids. It raises an important question—does the stability of well-organized structure of lipid bilayers upon dehydration depends more on the chemical structure of the lipid (and thus on some chemical properties), or is it mainly controlled by the phase transition of the membrane? To answer this

important question, we studied the structural stability of dehydrated DPPC:5-DSA membranes deposited inside AAO nanopores using EPR spectroscopy at 50°C, well above the gel-liquid phase transition temperature of 41°C.

As shown in Figure 3.9, raising the temperature to 50°C for full dehydrated DPPC membranes (no sugar added) resulted in a partial suppression of the Azz spectral features for AAO surface plane to be in perpendicular orientation with respect to magnetic field as compared to parallel orientation of the AAO surface plane. As discussed above, this provides direct evidence of the partial preservation of the membrane integrity and lipid alignment inside the membrane even in the absence of sugar. This is in sharp contrast to the same experiments done at room temperature (see section 3.2.1), well below the gel-liquid phase transition, where no membrane ordering was observed unless a sugar of smaller molecular size was added before dehydration.

These observations demonstrate that the phase transition of the lipid bilayer plays a critical role in maintaining membrane integrity inside AAO nanopores under fully dehydrated conditions. At this stage of the current study, it is difficult to judge if any other chemical properties of lipids might also play a role for maintaining the lipid alignment and membrane structural integrity. These interesting and important questions will be addressed in the future investigations being a continuation of the work presented.

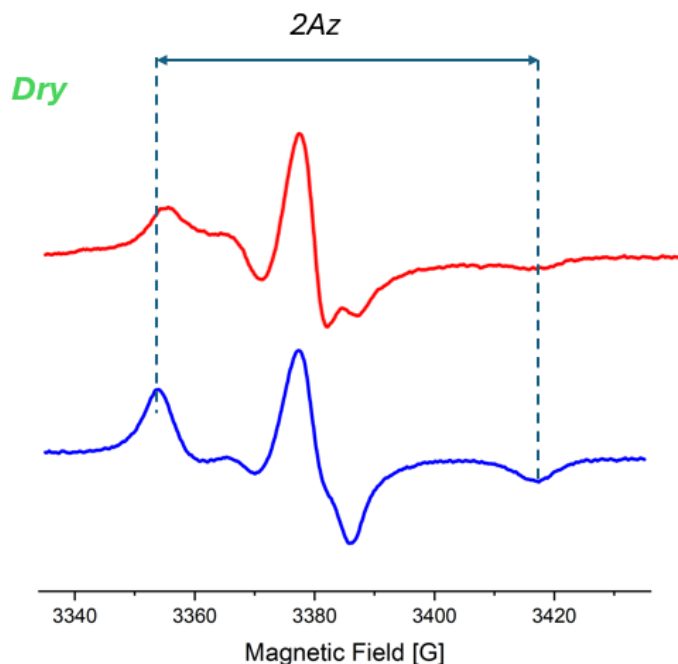


Figure 3.9 EPR (X-band) spectra of DPPC membranes labeled with 1 mol% 5-doxyl stearic acid (5-DSA) inside AAO are self-assembling with dehydration conditions including magnetic axis with DOXYL (g_{zz}) parallel (**blue spectrum**) and **perpendicular (red spectrum)** to the direction of the pore that is aligned along the external magnetic field at 50°C

3.5 Quantitative estimation of the structural order in dehydrated DOPC membranes using numerical simulations.

So far, in the previous sections, we judged the level of lipid alignment and degree of the membrane integrity based primarily on the intensity of the A_{zz} spectral features: the lower the intensity of the features, the higher the lipid alignment order and membrane integrity. The main drawback of such approach, however, is that it allows only for the qualitative estimation of the degree of structural order. It would be of high importance to develop an approach for the quantitative characterization of the order/disorder within a lipid membrane as described by some numerical values (order parameters). The approach we propose here is to use numerical simulations of the experimental

EPR spectra and obtain the order parameters by closest matching the simulated and experimental spectra. The simulation of such spectra is not a trivial task and generally requires both highly sophisticated numerical algorithms as well as high computation capacities. As series reasonable simplifications we will assume the following approximating conditions:

We will consider the 5-DSA not to have any rotational freedom i.e. each individual 5-DSA molecular moiety to have a fixed spatial orientation. This is probably reasonable for fully dehydrated sample where the rate of molecular motion should be slow enough not to significantly affect the EPR spectra.

We will consider that for the case when the AAO plane is parallel to the magnetic field, all possible molecular orientations of the lipids as well as 5-DSA moieties equiprobable i.e. all the observed 5-DSA spins have fully isotropic angular distribution. This is also quite reasonable, since for the parallel AAO plane all orientations are present. This combined with is a significant level of internal disorder within the lipids (even in an ideal case of a perfectly structurally intact membrane) should yield an angular distribution rather close to isotropic.

We will assume that the orientations of the magnetic tensors (g - tensor and A -tensor) are distributed according to Gaussian distribution. As a reference frame we will use the “laboratory frame” where z -axis is directed perpendicular to the AAO plane, y -axis is directed towards the center of a AAO pore as shown in the Figure 3.10. The orientation of each individual 5-DSA moiety can be described by three Euler angles: α , β , and γ . α corresponds to the rotation around z -axis, β corresponds to the rotation about the new y -axis (obtained after the first rotation) and γ corresponds to the rotation around the new z -axis (as shown in the Figure 3.10). We will consider the probabilities of these three angles to be Gaussian:

$$p(\alpha) = \frac{1}{\sqrt{2\pi}\sigma_\alpha} e^{-\frac{(\alpha-M_\alpha)^2}{2\sigma_\alpha^2}}$$

$$p(\beta) = \frac{1}{\sqrt{2\pi}\sigma_\beta} e^{-\frac{(\alpha-M_\beta)^2}{2\sigma_\beta^2}}$$

$$p(\gamma) = \frac{1}{\sqrt{2\pi}\sigma_\gamma} e^{-\frac{(\alpha-M_\gamma)^2}{2\sigma_\gamma^2}}$$

Where $M_\alpha, M_\beta, M_\gamma$ are the mean (average) values for the three Euler angle and $\sigma_\alpha, \sigma_\beta, \sigma_\gamma$ are the standard deviations of the three angles respectively.

In general, each of the Euler angles has to be considered in the interval from 0 to 360 degrees. However, EPR spectra have some important symmetry properties, described by the following equivalence relations:

$$\alpha \equiv \alpha + \pi$$

$$\beta \equiv -\beta$$

$$\gamma \equiv \gamma + \pi$$

By other words, EPR spectra for α and $\alpha+\pi$ are identical. The same is for β and $-\beta$ as well as for γ and $\gamma+\pi$. These three equivalence conditions reduce the overall computational complexity of the simulations by a factor of 8.

We have chosen the fully dehydrated DOPC lipids (without adding sugar) deposited inside AAO nanopores at room temperature as the system to apply the proposed approach for the quantitative estimation of the lipid alignment order.

As the first step, the spectrum for the case of the AAO plane to be parallel to the static magnetic field axis was simulated assuming isotropic orientations of the 5-DSA spins. The principal values of the g - and A -tensors were obtained by closely matching the simulated spectrum to the experimental one. Both simulated and experimental spectrum are shown in Figure 3.11. And the full set of g - and A -tensor principal components are given in Table 1.

As the second step, the obtained g - and A -tensor parameters were used to simulate the large set of multiple EPR spectra, where each individual EPR spectrum corresponds to each unique set of the three Euler angles.

As the final step, the EPR spectrum corresponding to the AAO plane perpendicular to the field orientation was obtained by the weighted integration over the entire large set of EPR spectra using three Gaussian distributions for the three Euler angles as weights for the integration. The six angular distribution parameters, namely M_α , M_β , M_γ and σ_α , σ_β , σ_γ were varied to obtain the closest possible match between the experimental and the simulated spectrum. The parameters corresponding to the best match are given in Table 2.

The three angular mean values M_α , M_β , M_γ characterize the preferred orientation of the magnetic tensors of 5-DSA moieties attached to the DOPC lipids. The three standard deviations, σ_α , σ_β , and σ_γ , can be considered as the parameters characterizing the degree of structural order of the lipid membrane.

From the values in Table 2, we can see the mean values of the first two Euler angles are close to 90 degrees: 76 and 100 degrees for α and β respectively. These set of angles correspond to an angle of 17 degrees between the g - and A -tensor z -axis and the vector normal to the membrane surface

i.e. the molecular magnetic z-axis is approximately collinear with the membrane normal. This agrees well with the earlier orientational EPR studies on DSA doped lipids [63].

Interestingly, standard deviations for the first and the third Euler angles (α and γ respectively) are rather small indicating high degree of structural order along these angular orientations. In contrast, the standard deviation for the second angle (β) was found to be very large indicating nearly complete disorder along this Euler angle orientation.

As can be seen from Figure 3.11, there are quite noticeable discrepancies between the simulated and experimental spectra for the perpendicular AAO plane orientation. The most probable reason for the disagreements is that in our model we assumed simple distributions (three independent Gaussian distributions in our case) for the Euler angles. While in real membranes, the angular distributions can be much more complex and not necessarily mutually independent. Thus, the presented quantitative approach should be considered as a highly approximating method for characterization of the lipid membrane degree of structural order (or alternatively disorder).

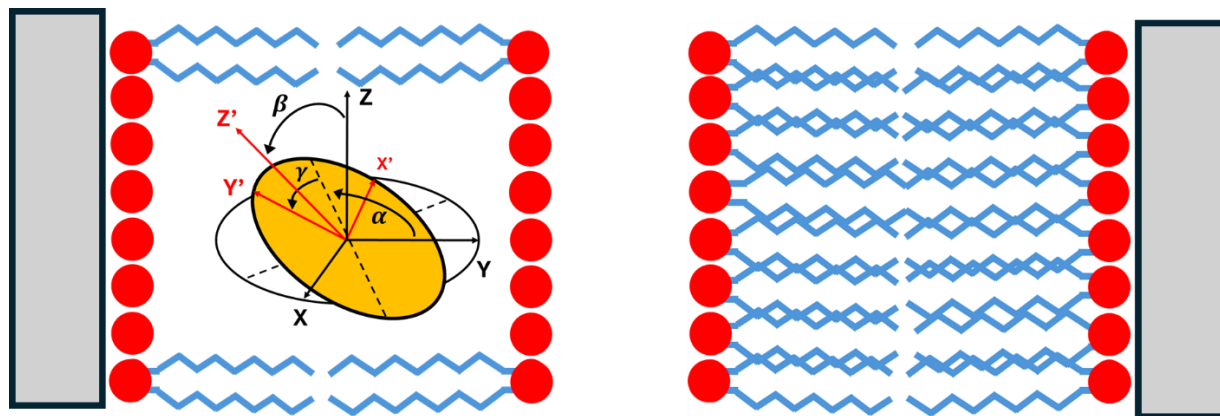


Figure 3.10: Orientation of the molecular frame defined by the g -tensor and A -tensor axes of 5-DSA radical with respect to the reference frame (axes denoted as X , Y , Z) within the lipid bilayer

inside the AAO nanopores. The orientation of the molecular frame is defined by three Euler angles (α, β, γ) , which were estimated by numerical simulations (see text for details).

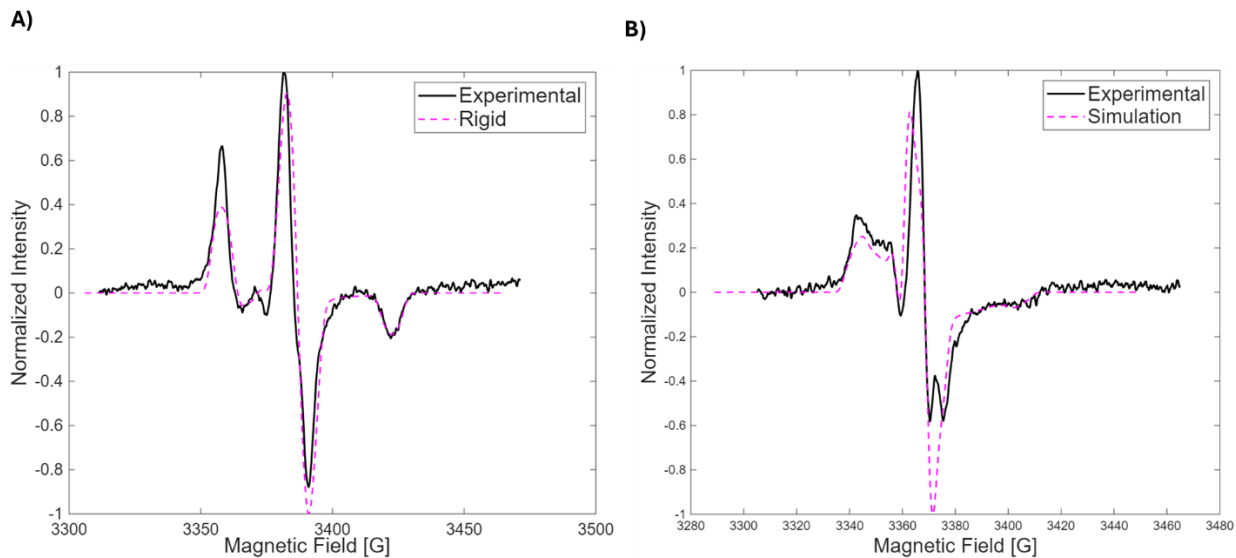


Figure 3.11: The normalized simulation (red dotted line) of DOPC membranes labeled with 1 mol% 5-doxy stearic acid (5-DSA) assembled within AAO fully dehydration at room temperature (23oC) which measured by X-band EPR spectroscopy (black solid line) with DOXYL (g_{zz}) A) parallel (blue spectrum) and B) perpendicular (red spectrum) to the direction of the pore that is aligned along the external magnetic field.

Table 1: Principal g - and A -Tensor components of 5-DSA obtained from spectrum simulation

g			A		
g_{xx}	g_{yy}	g_{zz}	A_x	A_y	A_z
2.0075	2.005	2.0025	4	4	32.2

Table 2: Angular orientation parameters ($M\alpha$, $M\beta$, $M\gamma$ and $\sigma\alpha$, $\sigma\beta$, $\sigma\gamma$) of 5-DSA in DOPC Membranes

	α	β	γ
M	76o	100o	170o
δ	15o	120o	10o

3.6 Probing the dehydrated DOPC membrane structure globally: DEER spectroscopy of Gramicidin A protein

Gramicidin is a linear pentadecapeptide antibiotic synthesized by the soil organism *Brevibacillus brevis*. It is a potent selective blocker of Gram-positive bacteria and has been the prototype ion channel studied for membrane biophysics applications. The presence of an alternating L-D amino acid sequence is responsible for its adoption of a β -helix conformation in lipid bilayers. Gramicidin has a 15-amino acid structure with eight left-handed and seven right-handed residues (Figure 3.12). [64], [65].

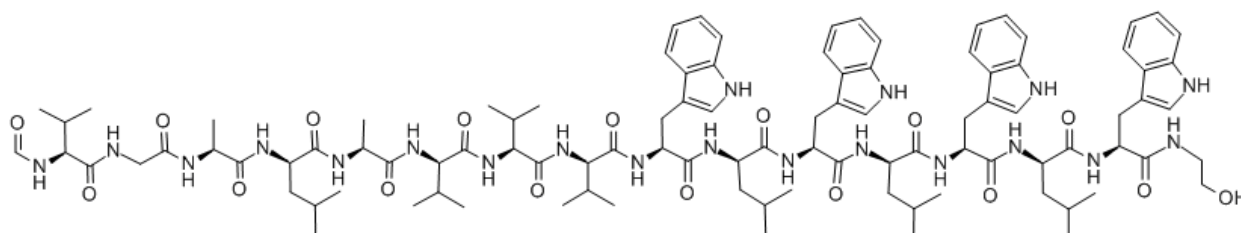


Figure 3.12: Gramicidin chemical structure

Upon insertion of gramicidin into a bilayer, such as DOPC, two monomers located in the opposed leaflets become paired head-to-head resulting in a dimeric channel that is ~ 26 Å long. This small

hydrophilic pore permits the passage of small monovalent cations (Na^+ , K^+) only, and not anions or larger ions [66]. Tryptophan residues positioned near the peptide termini anchor the channel at the lipid-water interface, which contributes to the stability and alignment of the dimer within the membrane. Advanced EPR studies often use reversible, site-directed spin labeling strategies to probe the structural organization of gramicidin channels. By attaching nitroxide spin-labels to the N-terminus, researchers can directly measure the distance between the labeled sites within a dimer, revealing the relative arrangement of subunits [67].

Pulsed dipolar spectroscopy and in particular DEER is among the most common and powerful methods to measure distances between spin labels on the scale of several nanometers (up to 8 nm generally). By chemically attaching electron spins to specific sites on gramicidin, we can measure the actual distance between monomers when they form a channel inside a membrane which reveal how the protein assembles and how its structure changes depending on the properties of the lipid bilayer [68], [69]. However, as we discussed in the previous sections, upon dehydration and below gel-liquid transition lipid membranes lose its structural order even being deposited inside such nanostructured materials as AAO. Luckily, as shown above we already found an effective way to preserve at least the local structure of a membrane by adding a small molecular size sugar such as Trehalose which replaces the missing water molecules upon membrane dehydration. Thus, it would be of great interest to probe the preservation of the global order and membrane functionality by measuring the inter-spin distances of a spin labelled Gramicidin A and comparing them to those known for the fully functional protein.

For this purpose, we measured DEER spectra of fully dehydrated DOPC lipids deposited inside AAO nanopores and containing Gramicidin A as well as Trehalose for two principal orientations of the AAO plane. The experimental time domain traces as well as their simulations obtained by

least square fitting procedure are shown in Figure 3.13. As can be seen from the figure, the simulations fit well the DEER trace when AAO plane orientation is parallel to the magnetic field axis and have significant discrepancy for the trace measured for the AAO plane perpendicular to the field direction. To understand the reason for this, it is important to note that in the simulations, all interspin vector orientations (vector connecting N-O groups of two spin labels within the ion channel) were assumed to be isotropic. As we discussed earlier, for AAO plane orientation parallel to the external magnetic field axis, the degree of orientation anisotropy is rather low, especially given that there is an unavoidable degree of local lipid orientational disorder even for a fully structurally undisturbed membrane. In this case, the numerical analysis provides reasonably accurate description of the experimental conditions, fits well to the measured trace and yields rather accurate distance distribution between the two spin labels, which is shown in Figure 3.13C. The obtained distance of ~ 2.7 nm and its width of ~ 0.7 nm (measured at half heights) agrees well with the previously reported values measured for DMPC membranes at their native hydration levels [70], [71]. This provides strong evidence of a structural integrity of the ion channel and thus preservation of the membrane functionality of the DOPC membranes deposited inside AAO nanopores under dehydration condition but protected by addition of small molecular size sugar, Trehalose.

Analysis of the DEER trace measured for perpendicular AAO orientation also provides very interesting results. Under the assumption of isotropic inter-spin vector orientations, the best fit is achieved by assuming extremely narrow distance distribution shown in Figure 3.13B. But even for this extremely narrow distance distribution, the damping of the dipolar modulations in the experimental trace is by far smaller than that of the simulated trace. In DEER damping of the modulations is directly related to the relative width of the distance distributions (i.e. ratio of the

width to the mean distance): the broader the distance distribution the faster the modulation damping. The reason why the observed damping is much slower than that simulated for an extremely (and unrealistically) narrow distribution is that inter-spin vector for the perpendicular AAO plane orientation is highly anisotropic with a strongly preferred orientation perpendicular to the magnetic field direction i.e. along the membrane normal. The obtained distance distribution in a combination with the observed orientation anisotropy (inter-spin vector being perpendicular to lipid normal) provide clear evidence of the preservation of global membrane integrity (at least on the scale of several nanometers along its surface) and its core functionality i.e. provide native environment for membrane proteins such as Gramidicin A. While Gramicidin A is a rather small protein, it would be of great interest to use a much larger sized membrane proteins as a probe of an order on a large scale.

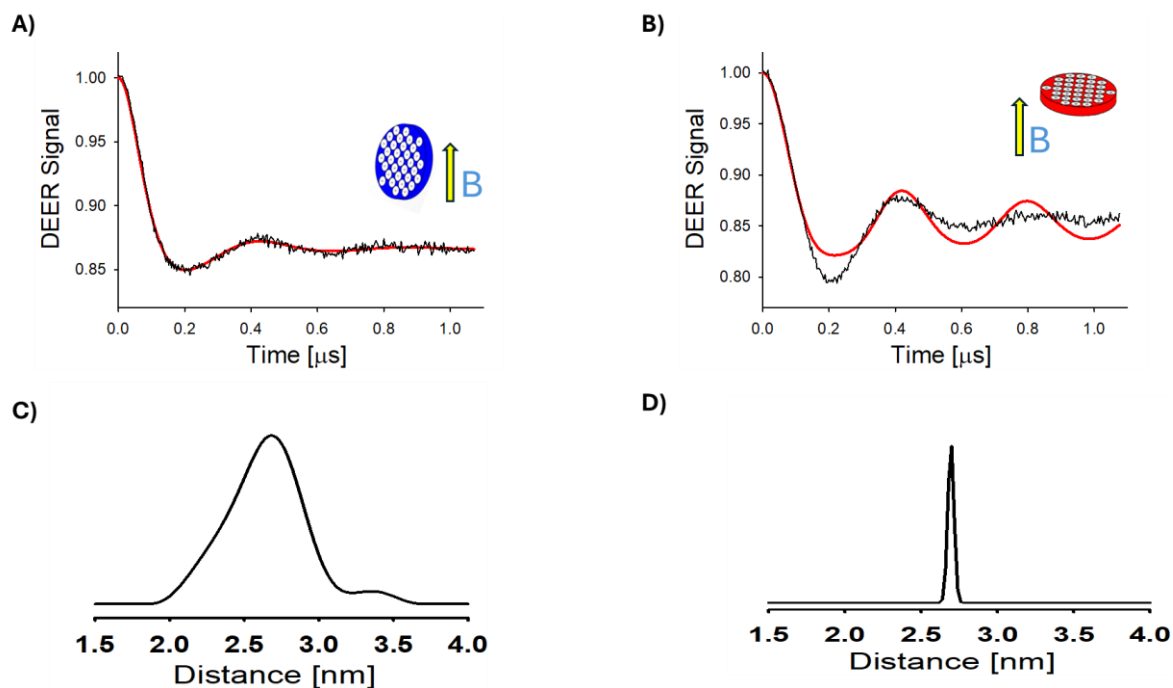


Figure 3.13: Q-band (34GHz) DEER spectroscopy of DOPC:Gramicidin A Membranes in AAO Nanopores with 20% Trehalose. Experimental A) and B) are DEER traces (black lines) measured at 76K for parallel and perpendicular AAO plane orientation with respect to magnetic field axis respectively. Red lines are the best fit by DEERAnalysys2019 using Tikhonov regularization and assuming isotropic inter-spin vector orientations in the sample. C) and D) are the distance distributions corresponding to the simulated traces shown in A) and B) respectively.

4. CONCLUSIONS

This study investigated the structural dynamics, alignment, and stability of lipid membranes confined within anodic aluminum oxide (AAO) nanopores using X-band EPR spectroscopy, controlled hydration, sugar additives, and DEER analysis. The results demonstrate that nanoconfinement in AAO provides a unique physical scaffold that preserves membrane order and enables controlled modulation of lipid behavior under otherwise destabilizing conditions.

Role of AAO in membrane structure stabilization

In contrast to bulk vesicles, DPPC membranes confined within AAO nanopores displayed clear macroscopic alignment, evidenced by orientation-dependent suppression of the A_{zz} hyperfine component. This alignment reflects direct templating of lipid bilayers by the cylindrical pore architecture, which constrains disorder and preserves structural orientation even across the DPPC gel-to-liquid crystalline transition.

Stability under dehydration and rehydration

While drying disrupted lipid alignment in the absence of additives, AAO confinement preserved a residual degree of order, preventing complete loss of orientation. Controlled rehydration revealed that AAO-stabilized membranes could progressively regain alignment at elevated humidity, underscoring the scaffold's role in maintaining a structural "memory" of ordered states that would otherwise be irreversibly lost.

Modulation by protective sugars

Trehalose further enhanced the stabilizing role of AAO by maintaining membrane alignment under fully dehydrated conditions. This cooperative effect reflects trehalose replacing hydration shells at lipid headgroups, while the AAO pores provide geometric constraints against large-scale disorder.

Ficoll, in contrast, failed to synergize with AAO, highlighting the specificity of sugar–lipid interactions in confined systems.

Dependence on lipid phase state

Comparative studies of DPPC and DOPC confirmed that confinement in AAO pores amplifies the inherent phase-dependent stability of membranes. DOPC retained partial alignment even when dry, whereas DPPC preserved order only when in the fluid phase at elevated temperature. Thus, AAO confinement couples with lipid phase properties to determine overall resilience.

Preservation of global membrane integrity

DEER experiments on gramicidin A demonstrated that AAO-confined, trehalose-stabilized membranes retain not only alignment but also protein-supporting functionality, with native-like inter-spin distances preserved under dehydration. This indicates that nanoconfinement protects both local lipid order and higher-level membrane architecture.

In summary, AAO nanoconfinement emerges as the primary stabilizing factor that enforces lipid alignment, restricts disorder, and preserves membrane structural integrity under environmental stress. Additives such as trehalose enhance this effect by chemically supporting headgroup hydration, but their protective action is secondary to the geometric templating provided by AAO. These findings establish nanoconfinement as a powerful physical principle for preserving ordered, functional membranes, with broad implications for membrane biophysics, nanostructured biointerfaces, and stabilization of membrane proteins in dry environments

5. REFERENCES

- [1] S. J. Singer and G. L. Nicolson, “The fluid mosaic model of the structure of cell membranes,” *Science*, vol. 175, no. 4023, pp. 720–731, Feb. 1972, doi: 10.1126/science.175.4023.720.
- [2] J. F. Nagle and S. Tristram-Nagle, “Structure of lipid bilayers,” *Biochimica et Biophysica Acta (BBA) - Reviews on Biomembranes*, vol. 1469, no. 3, pp. 159–195, Nov. 2000, doi: 10.1016/S0304-4157(00)00016-2.
- [3] P. R. Cullis and B. De Kruijff, “Lipid polymorphism and the functional roles of lipids in biological membranes,” *Biochimica et Biophysica Acta (BBA) - Reviews on Biomembranes*, vol. 559, no. 4, pp. 399–420, Dec. 1979, doi: 10.1016/0304-4157(79)90012-1.
- [4] O. G. Mouritsen, Ed., “Oil and Water,” in *Life — As a Matter of Fat: The Emerging Science of Lipidomics*, Berlin, Heidelberg: Springer, 2005, pp. 33–42. doi: 10.1007/3-540-27076-0_4.
- [5] “A Matter of Softness,” in *Life — As a Matter of Fat*, in The Frontiers Collection. , Berlin, Heidelberg: Springer Berlin Heidelberg, 2005, pp. 53–62. doi: 10.1007/3-540-27076-0_6.
- [6] D. M. Engelman, “Membranes are more mosaic than fluid,” *Nature*, vol. 438, no. 7068, pp. 578–580, Dec. 2005, doi: 10.1038/nature04394.
- [7] H. A. Rinia, M. M. Snel, J. P. van der Eerden, and B. de Kruijff, “Visualizing detergent resistant domains in model membranes with atomic force microscopy,” *FEBS Lett*, vol. 501, no. 1, pp. 92–96, July 2001, doi: 10.1016/s0014-5793(01)02636-9.
- [8] N. Kučerka, S. Tristram-Nagle, and J. F. Nagle, “Structure of Fully Hydrated Fluid Phase Lipid Bilayers with Monounsaturated Chains,” *J Membrane Biol*, vol. 208, no. 3, pp. 193–202, Jan. 2006, doi: 10.1007/s00232-005-7006-8.

- [9] D. P. Tieleman, S. J. Marrink, and H. J. Berendsen, “A computer perspective of membranes: molecular dynamics studies of lipid bilayer systems,” *Biochim Biophys Acta*, vol. 1331, no. 3, pp. 235–270, Nov. 1997, doi: 10.1016/s0304-4157(97)00008-7.
- [10] “The More We Are Together,” in *Life — As a Matter of Fat*, in The Frontiers Collection. , Berlin/Heidelberg: Springer-Verlag, 2005, pp. 91–103. doi: 10.1007/3-540-27076-0_10.
- [11] E. Sackmann, “Supported Membranes: Scientific and Practical Applications,” *Science*, Jan. 1996, doi: 10.1126/science.271.5245.43.
- [12] J. A. Killian, “Hydrophobic mismatch between proteins and lipids in membranes,” *Biochim Biophys Acta*, vol. 1376, no. 3, pp. 401–415, Nov. 1998, doi: 10.1016/s0304-4157(98)00017-3.
- [13] E. Perozo, A. Kloda, D. M. Cortes, and B. Martinac, “Physical principles underlying the transduction of bilayer deformation forces during mechanosensitive channel gating,” *Nat Struct Biol*, vol. 9, no. 9, pp. 696–703, Sept. 2002, doi: 10.1038/nsb827.
- [14] D. Marsh, “Orientation and Peptide–Lipid Interactions of Alamethicin Incorporated in Phospholipid Membranes: Polarized Infrared and Spin-Label EPR Spectroscopy,” *Biochemistry*, vol. 48, no. 4, pp. 729–737, Feb. 2009, doi: 10.1021/bi801279n.
- [15] K. Simons and D. Toomre, “Lipid rafts and signal transduction,” *Nat Rev Mol Cell Biol*, vol. 1, no. 1, pp. 31–39, Oct. 2000, doi: 10.1038/35036052.
- [16] “Lipids in Bilayers — A Stressful Life,” in *Life — As a Matter of Fat*, in The Frontiers Collection. , Berlin/Heidelberg: Springer-Verlag, 2005, pp. 81–89. doi: 10.1007/3-540-27076-0_9.

- [17] W. Rawicz, K. C. Olbrich, T. McIntosh, D. Needham, and E. Evans, “Effect of Chain Length and Unsaturation on Elasticity of Lipid Bilayers,” *Biophysical Journal*, vol. 79, no. 1, pp. 328–339, July 2000, doi: 10.1016/S0006-3495(00)76295-3.
- [18] O. G. Mouritsen, Ed., “Soft Shells Shape Up,” in *Life — As a Matter of Fat: The Emerging Science of Lipidomics*, Berlin, Heidelberg: Springer, 2005, pp. 63–71. doi: 10.1007/3-540-27076-0_7.
- [19] G. Zaccai, “How Soft Is a Protein? A Protein Dynamics Force Constant Measured by Neutron Scattering,” *Science*, June 2000, doi: 10.1126/science.288.5471.1604.
- [20] J. Israelachvili and H. Wennerström, “Role of hydration and water structure in biological and colloidal interactions,” *Nature*, vol. 379, no. 6562, pp. 219–225, Jan. 1996, doi: 10.1038/379219a0.
- [21] G. Pabst, “Structural information from multilamellar liposomes at full hydration: Full q -range fitting with high quality x-ray data,” *Phys. Rev. E*, vol. 62, no. 3, pp. 4000–4009, 2000, doi: 10.1103/PhysRevE.62.4000.
- [22] A. J. Sodt, M. L. Sandar, K. Gawrisch, R. W. Pastor, and E. Lyman, “The Molecular Structure of the Liquid-Ordered Phase of Lipid Bilayers,” *J. Am. Chem. Soc.*, vol. 136, no. 2, pp. 725–732, Jan. 2014, doi: 10.1021/ja4105667.
- [23] M. Caffrey, “Kinetics and mechanism of transitions involving the lamellar, cubic, inverted hexagonal and fluid isotropic phases of hydrated monoacylglycerides monitored by time-resolved x-ray diffraction,” *Biochemistry*, vol. 26, no. 20, pp. 6349–6363, Oct. 1987, doi: 10.1021/bi00394a008.
- [24] E. Reimhult, F. Höök, and B. Kasemo, “Intact Vesicle Adsorption and Supported Biomembrane Formation from Vesicles in Solution: Influence of Surface Chemistry, Vesicle

- Size, Temperature, and Osmotic Pressure,” *Langmuir*, vol. 19, no. 5, pp. 1681–1691, Mar. 2003, doi: 10.1021/la0263920.
- [25] H. Masuda and K. Fukuda, “Ordered metal nanohole arrays made by a two-step replication of honeycomb structures of anodic alumina,” *Science*, vol. 268, no. 5216, pp. 1466–1468, June 1995, doi: 10.1126/science.268.5216.1466.
- [26] R. C. Furneaux, W. R. Rigby, and A. P. Davidson, “The formation of controlled-porosity membranes from anodically oxidized aluminium,” *Nature*, vol. 337, no. 6203, pp. 147–149, Jan. 1989, doi: 10.1038/337147a0.
- [27] P. P. Mardilovich, A. N. Govyadinoy, N. I. Mazurenko, and R. Paterson, “New and modified anodic alumina membranes part II. Comparison of solubility of amorphous (normal) and polycrystalline anodic alumina membranes,” *Journal of Membrane Science*, vol. 98, no. 1, pp. 143–155, Jan. 1995, doi: 10.1016/0376-7388(94)00185-2.
- [28] W. Lee, R. Ji, U. Gösele, and K. Nielsch, “Fast fabrication of long-range ordered porous alumina membranes by hard anodization,” *Nature Mater*, vol. 5, no. 9, pp. 741–747, Sept. 2006, doi: 10.1038/nmat1717.
- [29] N. K. Chaki and K. Vijayamohanan, “Self-assembled monolayers as a tunable platform for biosensor applications,” *Biosens Bioelectron*, vol. 17, no. 1–2, pp. 1–12, Jan. 2002, doi: 10.1016/s0956-5663(01)00277-9.
- [30] A. P. Li, F. Müller, A. Birner, K. Nielsch, and U. Gösele, “Hexagonal pore arrays with a 50–420 nm interpore distance formed by self-organization in anodic alumina,” *Journal of Applied Physics*, vol. 84, no. 11, pp. 6023–6026, Dec. 1998, doi: 10.1063/1.368911.
- [31] S. K. Thamida and H.-C. Chang, “Nanoscale pore formation dynamics during aluminum anodization,” *Chaos*, vol. 12, no. 1, pp. 240–251, Mar. 2002, doi: 10.1063/1.1436499.

- [32] E. Y. Chekmenev, P. L. Gor'kov, T. A. Cross, A. M. Alaouie, and A. I. Smirnov, "Flow-Through Lipid Nanotube Arrays for Structure-Function Studies of Membrane Proteins by Solid-State NMR Spectroscopy," *Biophysical Journal*, vol. 91, no. 8, pp. 3076–84, Oct. 2006.
- [33] E. Sackmann, "Supported Membranes: Scientific and Practical Applications," *Science*, Jan. 1996, doi: 10.1126/science.271.5245.43.
- [34] Z. Siwy, "Fabrication of a Synthetic Nanopore Ion Pump," *Phys. Rev. Lett.*, vol. 89, no. 19, 2002, doi: 10.1103/PhysRevLett.89.198103.
- [35] C. R. Martin, "Membrane-Based Synthesis of Nanomaterials," *Chem. Mater.*, vol. 8, no. 8, pp. 1739–1746, Jan. 1996, doi: 10.1021/cm960166s.
- [36] L. J. Berliner and J. Reuben, Eds., *Spin Labeling: Theory and Applications*, vol. 8. in *Biological Magnetic Resonance*, vol. 8. Boston, MA: Springer US, 1989. doi: 10.1007/978-1-4613-0743-3.
- [37] W. L. Hubbell, D. S. Cafiso, and C. Altenbach, "Identifying conformational changes with site-directed spin labeling," *Nat Struct Mol Biol*, vol. 7, no. 9, pp. 735–739, Sept. 2000, doi: 10.1038/78956.
- [38] J. A. Weil and J. R. Bolton, *Electron Paramagnetic Resonance: Elementary Theory and Practical Applications*, 1st ed. Wiley, 2006. doi: 10.1002/0470084987.
- [39] J. H. FREED, "ESR Studies of Spin Probes in Anisotropic Media," in *Magnetic Resonance in Colloid and Interface Science*, vol. 34, in ACS Symposium Series, no. 34, vol. 34. , AMERICAN CHEMICAL SOCIETY, 1976, pp. 1–15. doi: 10.1021/bk-1976-0034.ch001.
- [40] H. M. McConnell and W. L. Hubbell, "Molecular motion in spin-labeled phospholipids and membranes," *J. Am. Chem. Soc.*, vol. 93, no. 2, pp. 314–326, Jan. 1971, doi: 10.1021/ja00731a005.

- [41] J. Seelig, “Spin label studies of oriented smectic liquid crystals (a model system for bilayer membranes),” *J. Am. Chem. Soc.*, vol. 92, no. 13, pp. 3881–3887, July 1970, doi: 10.1021/ja00716a008.
- [42] D. Marsh, “Electron spin resonance in membrane research: protein–lipid interactions from challenging beginnings to state of the art,” *Eur Biophys J*, vol. 39, no. 4, pp. 513–525, Mar. 2010, doi: 10.1007/s00249-009-0512-3.
- [43] M. Pannier, S. Veit, A. Godt, G. Jeschke, and H. W. Spiess, “Dead-Time Free Measurement of Dipole–Dipole Interactions between Electron Spins,” *Journal of Magnetic Resonance*, vol. 142, no. 2, pp. 331–340, Feb. 2000, doi: 10.1006/jmre.1999.1944.
- [44] E. L. Hahn, “Spin Echoes,” *Phys. Rev.*, vol. 80, no. 4, pp. 580–594, 1950, doi: 10.1103/PhysRev.80.580.
- [45] P. P. Borbat, E. R. Georgieva, and J. H. Freed, “Improved Sensitivity for Long-Distance Measurements in Biomolecules: Five-Pulse Double Electron–Electron Resonance,” *J. Phys. Chem. Lett.*, vol. 4, no. 1, pp. 170–175, Jan. 2013, doi: 10.1021/jz301788n.
- [46] G. Jeschke *et al.*, “DeerAnalysis2006—a comprehensive software package for analyzing pulsed ELDOR data,” *Appl. Magn. Reson.*, vol. 30, no. 3, pp. 473–498, June 2006, doi: 10.1007/BF03166213.
- [47] O. Schiemann *et al.*, “Benchmark Test and Guidelines for DEER/PELDOR Experiments on Nitroxide-Labeled Biomolecules,” *J. Am. Chem. Soc.*, vol. 143, no. 43, pp. 17875–17890, Nov. 2021, doi: 10.1021/jacs.1c07371.
- [48] D. Marsh and L. I. Horváth, “Structure, dynamics and composition of the lipid-protein interface. Perspectives from spin-labelling,” *Biochimica et Biophysica Acta (BBA) - Reviews*

- on *Biomembranes*, vol. 1376, no. 3, pp. 267–296, Nov. 1998, doi: 10.1016/S0304-4157(98)00009-4.
- [49] W. L. Hubbell, A. Gross, R. Langen, and M. A. Lietzow, “Recent advances in site-directed spin labeling of proteins,” *Current Opinion in Structural Biology*, vol. 8, no. 5, pp. 649–656, Oct. 1998, doi: 10.1016/S0959-440X(98)80158-9.
- [50] C. Altenbach, D. A. Greenhalgh, H. G. Khorana, and W. L. Hubbell, “A collision gradient method to determine the immersion depth of nitroxides in lipid bilayers: application to spin-labeled mutants of bacteriorhodopsin.,” *Proc Natl Acad Sci U S A*, vol. 91, no. 5, pp. 1667–1671, Mar. 1994, doi: 10.1073/pnas.91.5.1667.
- [51] H. S. Mchaourab, P. R. Steed, and K. Kazmier, “Toward the Fourth Dimension of Membrane Protein Structure: Insight into Dynamics from Spin-Labeling EPR Spectroscopy,” *Structure*, vol. 19, no. 11, pp. 1549–1561, Nov. 2011, doi: 10.1016/j.str.2011.10.009.
- [52] I. D. Sahu and G. A. Lorigan, “Site-Directed Spin Labeling EPR for Studying Membrane Proteins”, doi: 10.1155/2018/3248289.
- [53] B. G. Dzikovski, P. P. Borbat, and J. H. Freed, “Spin-Labeled Gramicidin A: Channel Formation and Dissociation,” *Biophysical Journal*, vol. 87, no. 5, pp. 3504–3517, Nov. 2004, doi: 10.1529/biophysj.104.044305.
- [54] N. Horasan, M. M. Sünnetçioğlu, and R. Sungur, “EPR spin label study of walnut oil effects on phosphatidylcholine membranes,” *Chemistry and Physics of Lipids*, vol. 140, no. 1, pp. 1–10, Apr. 2006, doi: 10.1016/j.chemphyslip.2005.12.004.
- [55] T. Ichimura, K. Doi, C. Mitsushashi, T. Ishida, and T. Nogami, “*meta*-Phenylene-bridged bis(imino nitroxide) biradicals as potential high-spin ligands,” *Polyhedron*, vol. 22, no. 14, pp. 2557–2564, July 2003, doi: 10.1016/S0277-5387(03)00299-7.

- [56] S. Weber, T. Wolff, and G. von Büнау, “Molecular Mobility in Liquid and in Frozen Micellar Solutions: EPR Spectroscopy of Nitroxide Free Radicals,” *Journal of Colloid and Interface Science*, vol. 184, no. 1, pp. 163–169, Dec. 1996, doi: 10.1006/jcis.1996.0607.
- [57] P. Labrude and C. Vigneron, “Stability and functional properties of haemoglobin freeze-dried in the presence of four protective substances after prolonged storage: dose-effect relationships,” *J Pharm Pharmacol*, vol. 35, no. 1, pp. 23–27, Jan. 1983, doi: 10.1111/j.2042-7158.1983.tb04257.x.
- [58] P. Wessman *et al.*, “Impact of matrix properties on the survival of freeze-dried bacteria,” *Journal of the Science of Food and Agriculture*, vol. 91, no. 14, pp. 2518–2528, 2011, doi: 10.1002/jsfa.4343.
- [59] C. Jh, C. Lm, and C. D, “Preservation of membranes in anhydrobiotic organisms: the role of trehalose,” *PubMed*, 1984, Accessed: Sept. 29, 2025. [Online]. Available: <https://pubmed.ncbi.nlm.nih.gov/17841031/>
- [60] S. B. Leslie, E. Israeli, B. Lighthart, J. H. Crowe, and L. M. Crowe, “Trehalose and sucrose protect both membranes and proteins in intact bacteria during drying,” *Appl Environ Microbiol*, vol. 61, no. 10, pp. 3592–3597, Oct. 1995, doi: 10.1128/aem.61.10.3592-3597.1995.
- [61] B. Kent, T. Hunt, T. A. Darwish, T. Hauß, C. J. Garvey, and G. Bryant, “Localization of trehalose in partially hydrated DOPC bilayers: insights into cryoprotective mechanisms,” *J R Soc Interface*, vol. 11, no. 95, p. 20140069, June 2014, doi: 10.1098/rsif.2014.0069.
- [62] M. Tang, A. J. Waring, and M. Hong, “Trehalose-Protected Lipid Membranes for Determining Membrane Protein Structure and Insertion,” *J Magn Reson*, vol. 184, no. 2, pp. 222–227, Feb. 2007, doi: 10.1016/j.jmr.2006.10.006.

- [63] A. I. Smirnov and O. G. Poluektov, "Substrate-Supported Lipid Nanotube Arrays," *J. Am. Chem. Soc.*, vol. 125, no. 28, pp. 8434–8435, July 2003, doi: 10.1021/ja0349406.
- [64] R. D. Hotchkiss and R. J. Dubos, "FRACTIONATION OF THE BACTERICIDAL AGENT FROM CULTURES OF A SOIL BACILLUS," *Journal of Biological Chemistry*, vol. 132, no. 2, pp. 791–792, Feb. 1940, doi: 10.1016/S0021-9258(19)56231-7.
- [65] R. Sarges and B. Witkop, "Gramicidin A. V. The Structure of Valine- and Isoleucine-gramicidin A," *J. Am. Chem. Soc.*, vol. 87, no. 9, pp. 2011–2020, May 1965, doi: 10.1021/ja01087a027.
- [66] D. A. Kelkar and A. Chattopadhyay, "The gramicidin ion channel: A model membrane protein," *Biochimica et Biophysica Acta (BBA) - Biomembranes*, vol. 1768, no. 9, pp. 2011–2025, Sept. 2007, doi: 10.1016/j.bbamem.2007.05.011.
- [67] B. A. Wallace, "Common structural features in gramicidin and other ion channels," *Bioessays*, vol. 22, no. 3, pp. 227–234, Mar. 2000, doi: 10.1002/(SICI)1521-1878(200003)22:3%3C227::AID-BIES4%3E3.0.CO;2-6.
- [68] B. G. Dzikovski, P. P. Borbat, and J. H. Freed, "Channel and non-channel forms of spin-labeled gramicidin in membranes and their equilibria," *J Phys Chem B*, vol. 115, no. 1, pp. 176–185, Jan. 2011, doi: 10.1021/jp108105k.
- [69] B. J. Wylie *et al.*, "Dynamic Nuclear Polarization of membrane proteins: covalently bound spin-labels at protein-protein interfaces," *J Biomol NMR*, vol. 61, no. 3–4, pp. 361–367, Apr. 2015, doi: 10.1007/s10858-015-9919-6.
- [70] S. Milikisiyants *et al.*, "Enhancing sensitivity of Double Electron-Electron Resonance (DEER) by using Relaxation-Optimized Acquisition Length Distribution (RELOAD)

scheme,” *Journal of Magnetic Resonance*, vol. 298, pp. 115–126, Jan. 2019, doi: 10.1016/j.jmr.2018.12.004.

- [71] B. G. Dzikovski, P. P. Borbat, and J. H. Freed, “Channel and non-channel forms of spin-labeled gramicidin in membranes and their equilibria,” *J Phys Chem B*, vol. 115, no. 1, pp. 176–185, Jan. 2011, doi: 10.1021/jp108105k.